Adiabatic Population Transfer Methods in Performing Quantum Computations and their Application with Femtosecond Pulses

by

Cian John Menzel-Jones

B.Sc., Queen's University, 2004

A THESIS SUBMITTED IN PARTIAL FULFILMENT OF
THE REQUIREMENTS FOR THE DEGREE OF

Master of Science

in

The Faculty of Graduate Studies

(Physics)

The University of British Columbia

October 2007

Abstract

This thesis is based upon the work published in the following two articles entitled: Robust Operation of a Universal Set of Logic Gates for Quantum Computation using Adiabatic Population Transfer between Molecular Levels [37], and Piecewise Adiabatic Passage with a Series of Femtosecond Pulses [54]. Both papers involve using the concept of a quantum control phenomenon, known as adiabatic passage in different manners, in order to achieve particular goals. In the first paper we present a robust construction of a set of logic gates operating on a system of qubits encoded in the ro-vibrational eigenstates of an Na_2 molecule using the optical Adiabatic Population Transfer (APT) method. We demonstrate the operation of a complete universal gate-set for quantum computation on a two-qubit system with gate fidelities approaching 99.99%. Like other APT-based processes, the method is robust against substantial fluctuations in the intensity of the laser pulse. Our construction is easily scalable to dealing with a larger number of qubits.

The second line of research developed from the desire to merge the robustness of an adiabatic process, as presented in the previous paper, with the speed and additional level of control available by using pulse shaping techniques of broadband pulses. Therein we develop a method of executing complete population transfers between quantum states in a piecewise manner using a series of femtosecond laser pulses. The method can be applied to a large class of problems as it benefits from the high peak powers and large spectral bandwidths afforded by femtosecond pulses. The degree of population transfer is found to be robust to a wide variation in the absolute and relative intensities, durations, and time ordering of the pulses. The method is studied in detail for atomic sodium where piecewise adiabatic population transfer, as well as the induction of Ramsey-type interferences, is demonstrated.

Table of Contents

List of Tables

List of Figures

Acknowledgements

I would foremost like to thank my supervisor Moshe Shapiro for his constant flow of new ideas and insightful advise that he past on to me throughout my research endeavors. He kept me intrigued with what seemed to be limitness possiblities for study stemming from his absolute love of the subject. I feel indebted for the interest he has instilled in me pervading from fundamental theoretical topics to practical experimental issues. Perhaps as important to my success has been the companionship of my colleagues Ioannis Thanopoulos and Evgeny Shapiro who have acted as teachers thoughout my studies. Their friendship allowed me to not be embarrassed by the answers to some of my most foolish of questions, but provided me with the space to discuss my own research ideas with confidence. Their honesty and sincerity made the days in the office inviting, even when work wasn't. I thank them for their opinions and suggestions in guiding me towards the future. More indirectly, I greatly appreciate the support that my family, specifically my parent, brother and sister, have provided me during this process. Their caring presence, although rarely physical, served as a comforting ground state and a reminder of a home away from the sciences. Lastly, but certainly not least importantly, I would like to thank Shannon for her love and encouragement, who made finishing work everyday something to look forward to.

to my parents

alan and elke

Chapter 1

Introduction

Since the development of quantum theory, researcher have sought for methods to probe and control quantum mechanical systems. Before the advent of wave amplification technology employing the quantum effect of stimulated emission radiation, a very limited amount could be achieved in this regard prominently due to the restrictiveness of the solely available interacting medium at the time, incoherent radiation. The introduction of maser/laser devices brought about a new found ability to produce an intense, nearly-monochromatic coherent electromagnetic field. This led to a theoretical reexamination of many previously known quantum effects and an explosion in the field of quantum methodology [8]. The application of coherent radiation to a quantum system produces effects which differ significantly from those that can be predicted by using Einstein's rate equation explaining incoherent irradiation. The new fundamental dynamical equation becomes the renown time-dependent Schrödinger equation which determines the time propagation of the quantum-mechanical wavefunction describing the system. The fact that there now existed a fixed (and controllable) phase relationship between all points in space and time of the electromagnetic field allowed for the phases of the wavefunction to maintain coherence during the course of the irradiation, which thus lead to the invention of more precise and sophisticated control techniques. The first section of Chapter 2 provides the reader with a quantitative description of both incoherent and coherent radiation as applied to an elementary model.

The primary objective in the majority of quantum control schemes involves guiding a system from some particular initial quantum state to another desired configuration. The simplest case often requires implementing a discrete bound-bound or bound-free transition between two eigenstates in an atom or molecule. Prior to the last few decades the methods

developed were, for the most part, concerned with usages in spectroscopy or in the photochemical control of molecular reactions. As a result most schemes thus created did not focus on acquiring perfect efficiency nor phase control of the quantum states. These control aspects changed amidst the revolution of the information age as the new field of quantum information was born. With the promise that certain computing algorithms, if implemented on a quantum mechanical system, could exponentially outperform their classical counterparts began an immense research campaign with groups in the quantum control field now moving their attention to the exciting new field of quantum computations. With new objectives in mind, namely the need for near perfect fidelity rates in manipulating state populations which can be facilitated by requiring schemes with a great robustness in experimental parameters, a review of old and a study of new control procedures ensued. The idea of utilizing an adiabatic evolution of a system in performing control operations became apparent as a natural choice for such environment sensitive applications. More specifically, the possibility of applying the phenomena known as adiabatic passage as a method for implementing highly efficient quantum logic operations as required for quantum computation, appeared worthy of research. The latter sections of Chapter 2 detail the two quintessential adiabatic passage schemes followed by a review of the basis concept of quantum computing. In Chapter 3 a procedure is developed for the application of performing certain logic operations of quantum information units encoded in a molecular system.

Despite the benefits of restricting a system to undergo an adiabatic evolution, there exist drawbacks that in some cases hinder the desired objective. For various applications it may not be possible nor advantageous to fit the laser parameters into the window of values required for adiabaticity. As a result it may be necessary to instate a complementary strategy to adiabatic passage for performing population transfer; known as coherent control. Coherent control can tailor itself to nearly any situation using a diverse range of laser techniques, however it suffers from an extreme sensitivity to the proper selection of the experimental parameters. Fortunately for the optical community, where each of these two methods fail the other triumphs, but does there exist a realm in which these coalesce? One

of the possible answers may be found in Chapter 4 in which exactly such an idea is realized along with a new regime for its applicability.

Throughout this thesis, the atomic and molecular systems of interest are treated entirely quantum mechanically, however the laser radiation (or light, since the wavelengths remain in the range of optical frequencies) permits a classical description. Apart from the onset, all excitations, which are restricted to bound state transitions, are assumed to occur by purely coherent radiation. This is an idealization that may, in practice, be tried by a variety of uncontrollable stochastic events, however it has been shown to be true to a good approximation [4]. All results of the numerical simulations were obtained by integrating the Schrödinger equation using a modified Verlet algorithm in FORTRAN code.

Note that unless otherwise specified atomic units ($\hbar = a_0 = m_e = e = 1$) are used throughout the text.

Chapter 2

Theory

2.1 Quantum Control

2.1.1 Incoherent Excitations

The first theory used to describe the interaction of a quantum mechanical system with a radiation field can be credited to Einstein. He considered the rates of change in the states' populations in a hypothetical ensemble of two-level atoms confined within a cavity [14]. Assuming that the cavity acts like a radiative blackbody saturating the containing particles by incoherent radiation with a frequency equal to the Bohr (transition) frequency of the atoms, we can write the following Markovian radiative rate equation

$$\frac{dP_j(t)}{dt} = \sum_i R_{j,i}(t)|c_j(t)|^2, \tag{2.1}$$

where $R_{j,i}(t)$ is a matrix of rate coefficients. Included in this matrix are the excitation and stimulated emission rates which he postulated to be proportional to the instantaneous radiation intensity $I(t) = |\mathcal{E}(t)|^2/8\pi$ times the Einstein-Milne B coefficient, and the spontaneous emission rate from the excited state, occurring at a rate A [59]. Assuming that all the atoms are initially at time $t \to -\infty$ in the ground state and that $BI \gg A$ (stimulated emission dominates the spontaneous emission), then the excited-state population at time t is given by

$$P_{ex}(t) = \frac{1}{2}(1 - e^{-B\int_{-\infty}^{t} I(t')dt'}). \tag{2.2}$$

From the above equation it can be seen that the population-transfer efficiency increases as a function of the duration and intensity of radiation. However, over a sufficiently long period of time this value asymptotically reaches 50% - the maximum possible excitation efficiency using incoherent light.

In practice, even achieving this population transfer efficiency is difficult, particularly when dealing with a realistic multilevel system where the assumptions of a thermodynamic equilibrium between the state populations and a broadband isotropic field are no longer valid. Despite the outlook, there do exist schemes, such as optical pumping or stimulated emission pumping, which are sufficient for various spectroscopic applications, but their efficiencies rarely operate above 10% [72]. To obtain superior results we need to exploit the properties of coherent radiation, which can be quantitatively described using traditional quantum mechanics.

2.1.2 Coherent Population Transfer

Preliminaries

In quantum mechanics we can express the state of a system, described by a time-independent Hamiltonian H_0, using a state vector

$$|\Psi(t)\rangle = \sum_{j=1}^{N} c_j'(t)|j\rangle = \sum_{j=1}^{N} c_j(t)|j\rangle e^{-i\xi_j(t)} , \tag{2.3}$$

where

$$H_0|j\rangle = E_j|j\rangle \quad \forall \quad j = \{1,..,N\}. \tag{2.4}$$

Each of the eigenvectors $|j\rangle$ of H_0 are associated with one of the N allowable energy levels of the system given by its corresponding eigenvalue E_j. The complex-valued coefficients $c_j'(t)$ are the time-dependent probability amplitudes whose absolute squares provide the probabilities $P_j(t) = |\langle\phi_n|\Phi(t)|^2 = |c_j'(t)|^2 = |c_j(t)|^2$ of finding the system at time t in the state $|j\rangle$. These probabilities will also be known as the *population* of a given state.

The value of the phase factors $\exp(-i\xi_j(t))$ extracted from the $c_j'(t)$ coefficients in Eq.(2.3) can, in general, be arbitrary chosen, unless we desire to prepare our system in a particular coherent superposition state. Often, this additional gauge freedom can be used to simplify the mathematical construction of certain problems through a suitable selection of $\xi_j(t)$.

Governing the evolution of a state vector, $|\Psi(t)\rangle$, is the time-dependent Schrödinger equation (TDSE)

$$i\frac{d|\Psi(t)\rangle}{dt} = H(t)|\Psi(t)\rangle \ , \tag{2.5}$$

where $H(t)$ is the total Hamiltonian of the system. In a non-interacting, time-independent system we obtain the stationary state solutions on the TDSE given by

$$|\Psi(t)\rangle = \sum_{j=1}^{N} c_j(t)|j\rangle e^{-iE_j(t)}. \tag{2.6}$$

As expected, the probability density, $|\langle\Psi(t)|\Psi(t)\rangle|^2$, and the expectation value, $\langle\Psi(t)|\hat{\mathrm{O}}|\Psi(t)\rangle$, of any observable $\hat{\mathrm{O}}$, remain fixed as a function of time. Over time each state only acquires a *dynamical* phase, which is related to its energy. If the gauge is fixed to correspond to this solution, ie. $\xi_j(t)) = E_j t$, then we are said to be in the Dirac picture (or interaction representation). For many situations this choice is convenient since the coefficients, $c_j(t)$, remain constant in the absence of any forces acting on the system. Although this exponential phase factor typically does not affect population transfer schemes it must be kept track of later when we begin to deal with quantum computations.

To determine the behavior of an atomic (or interchangeably molecular) system subject to an electromagnetic field, an additional term $V(t)$ defining its interaction with the field is added to the static system Hamiltonian H_0. The dominant components of this matter-radiation interaction term depends on the type of fields involved and the specific structure of our system. In this thesis we will be solely concerned with the response of a quantum system to *laser* radiation. It is useful to approximate laser fields by a linearly polarized plane wave, and then consider its interactions with an atom. Here we will define the field

to be a traveling wave, propagating in the x-direction with a frequency ω, defined as

$$\mathbf{E}(\mathrm{r},t) = \mathcal{E}(t)cos(kx-\omega t)\hat{\mathbf{z}} \quad \mathbf{B}(\mathrm{r},t) = -\mathcal{E}(t)cos(kx-\omega t)\hat{\mathbf{y}}\,, \tag{2.7}$$

where $k = 2\pi/\lambda$ is the wave vector and λ represents the wavelength. The field amplitude $\mathcal{E}(t)$ may be constant for continuous-wave lasers or for pulsed light may commonly be defined by a time-dependent Gaussian or sine-squared profile. When impinging upon an atomic system these waves act on the various multi-pole moments of the atom; the most prominent being the electric and magnetic, dipole and quadrupole interactions. For the particular excitations we are interested in, the frequencies used will be in the optical region of the spectrum which have wavelengths much larger than the dimensions of any small molecule. As a result the interactions will be largely dominated by the electric dipole terms (by an order of $\alpha/2 = 1/274$ [59]) known as E1 interactions. Using the *dipole approximation* the potential associated with the magnetic field and higher order electric multi-polar terms will be omitted from $V(t)$ in favor of a spatially uniform electric field $\mathbf{E}(\mathbf{r},t)$ acting on the electric dipole moment, $\boldsymbol{\mu}$, of the atom, which is defined as

$$\boldsymbol{\mu} = \int d^3r\rho(\boldsymbol{r})\boldsymbol{r}\,. \tag{2.8}$$

In quantum-mechanical systems, the continuous charge distribution $\rho(\boldsymbol{r})$ is the electron charge $(-e)$ times the probability of observing an electron at a position $\boldsymbol{r}$, which is usually defined relative to the center of mass of the atom. The interaction energy will thus be written as

$$V(t) = V^{E1}(t) \equiv -\boldsymbol{\mu}\cdot\mathbf{E}(t). \tag{2.9}$$

where the electric field

$$\mathbf{E}(t) = \mathcal{E}(t)cos(\omega t+\phi)\hat{\mathbf{e}} \tag{2.10}$$

has been idealized to be a nearly monochromatic field of frequency ω, with amplitude $\mathcal{E}(t)$ and polarization direction $\hat{\mathbf{e}}$, at the location of the atom. A phase can also be given to the

electric field, which is denoted here by ϕ. The vector $\boldsymbol{\mu}$, also known as the *transition dipole moment operator*, will naturally depend upon the specific state of the atom or molecule. The strength of an electric-dipole induced transition is quantitatively described by the matrix elements between two bound states $|j\rangle$ and $|k\rangle$

$$\mu_{j,k} \equiv \langle k|\boldsymbol{\mu} \cdot \hat{\mathbf{e}}|j\rangle. \tag{2.11}$$

To understand the effect of these matrix elements on specific transitions between states, we will consider a hypothetical two-level quantum system and study its behavior in the presence of laser light.

Two States

Suppose there exist two non-degenerate levels, denoted by $|0\rangle$ and $|1\rangle$, which represent the ground and excited state of some atom. These states represent the eigenstates of some unperturbed Hamiltonian, H_0, of the system with eigenvalues E_0 and E_1 respectively. Prior to any perturbation from a laser field the population is assumed to lie entirely in the ground state, i.e., $|c_0|^2 = 1$. The total Hamiltonian upon applying an electric field $\mathbf{E}$(t) is given by

$$H(t) = H_0 - \boldsymbol{\mu} \cdot \mathbf{E}(t). \tag{2.12}$$

Substituting the state-vector expansion of Eq. (2.3) into the TDSE with the above Hamiltonian gives us a set of coupled first-order ordinary differential equations

$$\frac{d\mathbf{c}(t)}{dt} = -i\mathbf{H}(t)\mathbf{c}(t), \tag{2.13}$$

where $\mathbf{c}(t) = [c_0, c_1]^T$ is a vector of time-dependent probability amplitudes and $\mathbf{H}(t)$ is a 2x2 Hamiltonian matrix whose elements depends on the choice of phases in Eq. (2.3). If we decide to adopt the Schrödinger picture, where the phases $\xi_j(t) = 0 \; \forall \; j$, then the diagonal matrix elements of $\mathbf{H}(t)$ would equal the energies E_j of the two states, and the off-diagonal

elements would hold the electric-dipole interaction energy. Although this is the most natural representation, mathematically it proves much easier to move into a rotating references frame in the two-dimensional Hilbert space governed by the carrier frequency of the field, ω. In this *rotating-wave picture* these phases are set to $\xi_0(t) = E_0 t$ and $\xi_1(t) = \xi_0(t) + \omega t + \phi$, where ϕ is the phase of the laser field appearing in Eq. (2.10) which we set to zero. In this representation the matrix elements of the Hamiltonian can be simplified by applying the *rotating-wave approximation* (RWA) giving

$$\mathbf{H}(t) = \begin{pmatrix} 0 & \frac{1}{2}\Omega_{0,1}(t) \\ \frac{1}{2}\Omega^*_{1,0}(t) & \Delta(t) \end{pmatrix}. \tag{2.14}$$

The single diagonal element $\Delta(t) = \omega_{10} - \omega(t)$ represents the detuning of the carrier frequency $\omega(t)$ from that of the energy difference $\omega_{10} = E_1 - E_0$. Parameterizing the strength of the interaction between the two levels is the *Rabi frequency* $\Omega(t)$ which is defined as

$$\Omega_{i,j}(t) = \mu_{i,j}\mathcal{E}(t). \tag{2.15}$$

In the off-diagonal elements, where the RWA amounted to replacing $(1 + exp(2i\omega t)) \approx 1$, it was assumed the exponential undergoes many oscillations before any significant changes in the coefficients c_j occur. Provided the dominant effects on the system take place over many optical cycles ω, the higher frequency components can be time-averaged over a single optical cycle, leaving only the effects of interest. Additionally for this approximation to remain valid, one must use near-resonant ($\Delta(t) \ll \omega(t)$) weak-field ($|\Omega_{0,1}(t)| \ll \omega(t)$) radiation coupling the two states

Similar to the incoherent rate equations, there exist an analytic solution for this two-state coherent excitation. In this case the excitation probability can be written as

$$P_1(t) = \frac{1}{2}R(1 - cosA(t)) \ , \tag{2.16}$$

where

$$R = \left(\frac{\Omega}{\tilde{\Omega}}\right)^2 , \qquad A(t) = \tilde{\Omega}t . \tag{2.17}$$

The argument in the cosine, $A(t)$, is known as the pulse area; here it is a function of the non-resonant flopping frequency $\tilde{\Omega} = \sqrt{\Omega^2 + \Delta^2}$, omitting the time dependence and $\{i, j\}$ subscripts for simplicity. Eq. (2.16) indicates that the application of perfectly resonant light ($\Delta = 0$) will cause complete sinusoidal oscillations of the state populations (i.e. Rabi oscillations) with a frequency of $\tilde{\Omega}(t)$. As the detuning is increased the amplitude of these oscillations, R, diminish and the oscillation frequency becomes more rapid between levels. Notice that if $A(t) = (2n+1)\pi$ for any $n \epsilon I$, complete population transfer can be achieved from states $|0\rangle \rightarrow |1\rangle$. Thus, by precisely specifying the laser intensity and duration we can control exactly the occupation of two levels for a given dipole coupling. Unfortunately, when dealing with real atomic or molecular systems the interaction strength may depend strongly on the orientations and trajectories of the particles involved. For example, in the case where the 'target' (excited) state is one of several magnetic sub-levels m of an atom or molecule, the Rabi frequency coupling the initial and final states is dependent upon the orientation of the dipole moment $\mu_{0,m}$ relative to the polarization direction of the electric field. Also, due to the finite cross-section of the laser beam, particles with transverse trajectories may be subject to varying intensities of the electric field. In addition, those particles with motion in the parallel direction relative to the traveling wave, will exhibit a Doppler shift of the carrier frequency, resulting in a detuning from the exact resonance. Since these effects cause variations in the pulse area, using the common π-pulse approach to perform a complete population transfer between two states is not realistic for many applications. Could a slightly different analysis of the simple two-state system yield a superior alternative?

Adiabatic Passage

In the previous discussion of the two-state system, the unperturbed eigenstates states $|j\rangle$ were used to represent the state of the atom throughout the interaction. However, any two

states which form a basis for the Hilbert space can be used as a valid representation of the state of the system. In particular, it proves useful to consider a time-dependent basis $|\lambda_k(t)\rangle$ in a moving coordinate system which are instantaneous eigenstates of the evolving Hamiltonian of Eq. (2.14):

$$\mathbf{H}(t)|\lambda_k(t)\rangle = \lambda_k(t)|\lambda_k(t)\rangle. \tag{2.18}$$

Here the eigenvectors $|\lambda_k(t)\rangle$, also known as dressed or adiabatic states, can be expressed in terms of the unperturbed (or bare or diabatic) basis states as

$$\begin{aligned} |\lambda_+(t)\rangle &= \sin\Theta(t)|0\rangle + \cos\Theta(t)|1\rangle \ , \\ |\lambda_-(t)\rangle &= \cos\Theta(t)|0\rangle - \sin\Theta(t)|1\rangle \ , \end{aligned} \tag{2.19}$$

where, by definition, the mixing angle is

$$\Theta(t) \ (\mathrm{mod}\ \pi) \equiv \frac{1}{2}\arctan\left(\frac{|\Omega(t)|}{\Delta(t)}\right) \ , \tag{2.20}$$

and the $\lambda_k(t)$ of $\mathbf{H}(t)$, representing the energies of the two adiabatic states, are given by

$$\lambda_\pm(t) = \frac{1}{2}\left(\Delta(t) \pm \sqrt{\Delta^2 + |\Omega(t)|^2}\right). \tag{2.21}$$

The advantage of expanding the total wavefunction $\Phi(t)$ in this rotating basis becomes apparent if we restrict the Hamiltonian to undergo an *adiabatic evolution.* This requires that the energy gap between the adiabatic states be must larger than their coupling,

$$|\lambda_+ - \lambda_-| \gg |\langle\dot{\lambda}_+|\lambda_-\rangle| \ . \tag{2.22}$$

In this context we may rewrite the above adiabaticity condition as

$$\left(|\Omega|^2 + \Delta^2\right)^{\frac{3}{2}} \gg \frac{1}{2}|\dot{\Omega}\Delta - \Omega\dot{\Delta}| \ , \tag{2.23}$$

where the dot($\dot{}$) represents the time derivative. Hence, the Rabi frequency and the detuning must change sufficiently slowly over the duration of the interaction. In practice, this amounts to using a typical pulse area $A \approx 10$. If these conditions are met, then the adiabatic theorem states that there will be no interactions between the adiabatic states and that their populations will remain conserved [25]. As the adiabatic states move relative to the bare basis $|j\rangle$, the wavefunction $\Phi(t)$ will appear fixed in the time-varying coordinate system, while its projection onto the bare basis states changes.

Suppose an adiabatic state is uniquely identified at $t \to -\infty$ with the initial bare eigenstate $|0\rangle$ (in which the system rest) and then later as $t \to \infty$ with an excited bare state $|1\rangle$. Then, provided that the Hamiltonian evolved adiabatically, we should expect the population to remain trapped in that particular adiabatic state which thus allows the population to transfer smoothly between the two bare states. In our two-level system considered here we can achieve such a process by letting the detuning $\Delta(t)$ sweep slowly across the resonance from a 'large' negative to a 'large' positive value, where 'large' implies $\Delta \gg \Omega(t)$. As a result the mixing angle $\Theta(t)$ will rotate from an initial value $\Theta(-\infty) = \pi/2$ to a final position $\Theta(+\infty) = 0$ over the course of the laser interaction. From Eqs. (2.19) we obtain the sought after asymptotic connections

$$|\lambda_+(t)\rangle \to \begin{cases} |0\rangle & \text{if t} \to -\infty \\ |1\rangle & \text{if t} \to \infty. \end{cases} \tag{2.24}$$

This process by which the population in an initial ground state, $|0\rangle$, moves adiabatically through a superposition state during the interaction and into a final state, $|1\rangle$, is known as adiabatic passage (AP). The advantage of AP over the previous coherent control scheme (π-pulse) is its inherent robustness to the pulse parameters; fluctuations in the laser intensity, detuning and duration do not affect the complete population transfer, provided that the adiabatic conditions are satisfied. This concept of 'trapping' population to an adiabatic states and then connecting initial and target levels can also be extended to multi-state

systems, where in certain situations the basis 2-level AP process is not possible and more sophisticated schemes must be developed.

2.1.3 AP in Three-Level Systems

In a realistic atomic or molecular system, single-photon transitions between certain levels may be ruled out by selection rules. If a population transfer between such states is desired, other methods must be considered which rely on incorporating in the other levels into the interaction dynamics. Some available control procedures such as the two-photon π-pulse, the three-level *pump-dump* scheme or stimulated emission pumping (SEP) [4] have problems in either their ability to obtain complete population transfers or their high sensitivity to experimental parameters.

The *pump-dump* method, which uses an *intermediate* level to which both initial and target levels can radiatively couple, works through the application of two successive π-pulses. The first, the *pump* field, moves the population to an intermediate state, and a second, the *dump* (or *Stokes*) pulse, transfers that population to its destination. Here the area of both pulses must be precisely defined and the spontaneous emission (decay) rate from the intermediate state must be sufficiently low for a transfer to be successful. Surprisingly, better efficiency can by attained if the two fields are applied in a *counter-intuitive* order, where the Stokes field precedes the pump. This is provided that certain conditions are met, namely that there exist enough overlap between the fields and that each field maintains a sufficiently large area. This scheme, which is based on AP, takes advantage of the coherence of two pulsed laser fields and avoids problems associated with the other methods, has become known as stimulated Raman adiabatic passage (STIRAP).

Stimulated-Raman Adiabatic Passage

The STIRAP technique will be discussed here in the context of a three level Λ-system system as shown in Fig. 2.1. The objective is to completely transfer the population from the ground state $|0\rangle$ to the unpopulated excited state $|1\rangle$ to which it can not be directly coupled. The

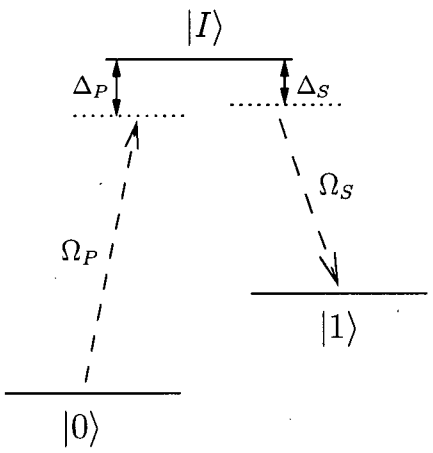

Figure 2.1: Interaction scheme of a typical STIRAP on a system of three levels in the Λ configuration.

pump and Stokes fields, denoted by Ω_P and Ω_S respectively, couple each level to a vacant intermediate level, $|I\rangle$, which may spontaneously decay to any available state of the atom. The single-photon detunings of the two central frequencies ω_P and ω_S of the pulses are defined by

$$\Delta_P = E_I - E_0 - \omega_P \ , \ \text{and} \ \Delta_S = E_I - E_1 - \omega_S \ , \tag{2.25}$$

where E_j for $j = \{0, 1, I\}$ represent the energies of the states. These single-photon detunings have relatively small effect on STIRAP, provided the crucial two-photon resonance condition is maintained:

$$\delta \equiv \Delta_P - \Delta_S = 0. \tag{2.26}$$

For this system the Hamiltonian in the RWA

$$\mathbf{H}(t) = \frac{1}{2} \begin{pmatrix} 0 & 0 & \Omega_P(t) \\ 0 & 2\delta & \Omega_S(t) \\ \Omega_P^*(t) & \Omega_S^*(t) & 2\Delta_P \end{pmatrix}, \tag{2.27}$$

satisfies Eq. (2.13) for the three-component vector $\mathbf{c(t)} = (c_0, c_1, c_I)^T$. The Rabi frequencies are defined similar to Eq. (2.15) and the fields here are assumed to have zero additional

phase ϕ. Solving for the instantaneous eigenstates (adiabatic states) of $\mathbf{H}(t)$, as in Sec. 2.1.2 we obtain the relations

$$\begin{aligned} |\lambda_+(t)\rangle &= \sin\vartheta(t)\sin\varphi(t)|0\rangle + \cos\vartheta(t)\sin\varphi(t)|1\rangle + \cos\varphi(t)|I\rangle \\ |\lambda_0(t)\rangle &= \cos\vartheta(t)|0\rangle - \sin\vartheta(t)|1\rangle \\ |\lambda_-(t)\rangle &= \sin\vartheta(t)\cos\varphi(t)|0\rangle - \cos\vartheta(t)\sin\varphi(t)|1\rangle + \sin\varphi(t)|I\rangle \end{aligned} \tag{2.28}$$

where the two mixing angles are defined as

$$\vartheta(t) \pmod{\pi} \equiv \arctan\left(\left|\frac{\Omega_P(t)}{\Omega_S(t)}\right|\right), \tag{2.29}$$

$$\varphi(t) \pmod{\pi} \equiv \frac{1}{2}\arctan\left(\frac{\sqrt{|\Omega_S(t)|^2 + |\Omega_P(t)|^2}}{\Delta_P(t)}\right). \tag{2.30}$$

Suppose we apply the counter-intuitive pulse ordering, where at early times it is assumed that only the Stokes pulse is present while at much later times only the pump pulse remains. By looking at the behavior of the adiabatic states at the two time extrema, summarized in Table 2.1 for the case of zero detuning, we see that the $|\lambda_0(t)\rangle$ state connects the initial level with the desired final state.

	$t \to -\infty$	$t \to \infty$
$\vartheta(t)$	0	$\frac{\pi}{2}$
$\varphi(t)$	$\frac{\pi}{4}$	$\frac{\pi}{4}$
$\|\lambda_0(t)\rangle$	$\|0\rangle$	$-\|1\rangle$
$\|\lambda_+(t)\rangle$	$\frac{1}{\sqrt{2}}(\|I\rangle + \|1\rangle)$	$\frac{1}{\sqrt{2}}(\|0\rangle + \|I\rangle)$
$\|\lambda_-(t)\rangle$	$\frac{1}{\sqrt{2}}(-\|I\rangle + \|1\rangle)$	$\frac{1}{\sqrt{2}}(\|0\rangle - \|I\rangle)$

Table 2.1: Temporal extremum values of the mixing angles and adiabatic states in a three-level Λ-system STIRAP.

Since neither of the other two adiabatic states $|\lambda_\pm\rangle$ have a $|0\rangle$ state component at early times when only the Stokes pulse is present, the state vector gets projected entirely onto $|\lambda_0\rangle$. As the dump field slowly increases, the population remains in the *trapped* state $|\lambda_0\rangle$ and gets smoothly transfered to the final state $|1\rangle$. The adiabatic eigenvector which conducts

this adiabatic passage has a zero eigenvalue, and thus does not acquire a dynamical phase contribution throughout its evolution. As a result it is called a *null* state. Since the evolution must remain adiabatic, the electric field must obey certain conditions similar to those of Eq. (2.22). To simplify the situation the pump and Stokers fields are both assumed to be typical Gaussian pulses with a width τ and the same peak Rabi frequency Ω_{max}. The optimum transfer occurs by maximizing the adiabaticity of the process with respect to the following parameters: Ω_{max}, τ and d, the delay between pulses. Typically, whenever the values

$$\Omega_{max} \geq 10 \quad \text{and} \quad \mathrm{d} \approx \tau \tag{2.31}$$

we retain adiabaticity and STIRAP works effectively [4]. As will be shown later, moderate fluctuations in the pulse parameters, and even large changes in the region of overlapping pulses, do not significantly affect the transfer efficiency.

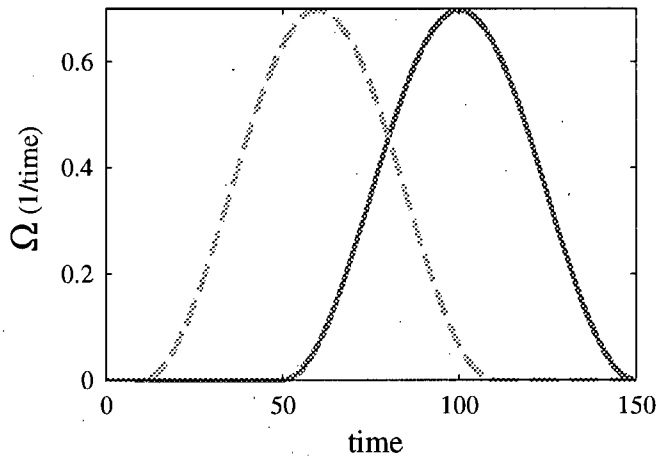

Figure 2.2: (a)

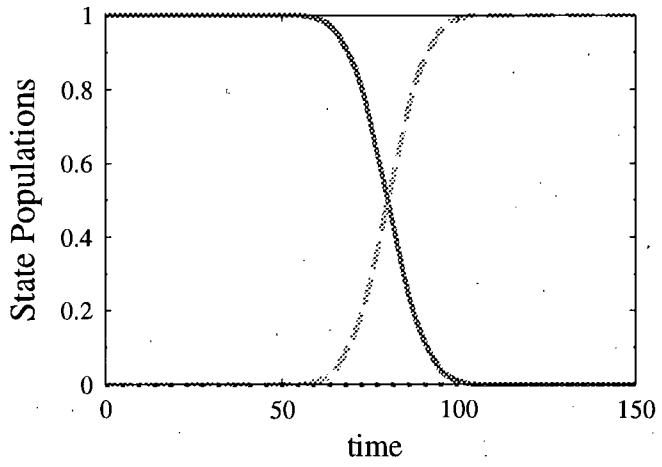

Figure 2.2: (b)

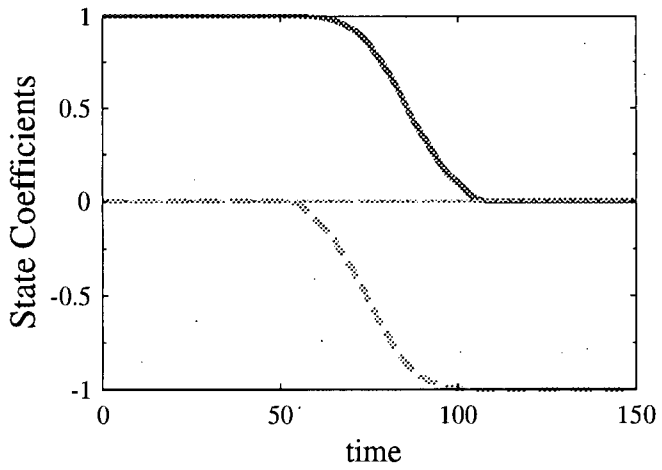

Figure 2.2: (c)

Figure 2.2: A sample simulation of STIRAP on a three-level Λ-system. Time is given in arbitrary units. (a) Temporal profile of the pump and Stokes Rabi frequencies shown by solid and dashed lines respectively. (b) Evolution of the three states population: $|0\rangle$ (solid line), $|1\rangle$ (dashed line) and $|I\rangle$ (dotted line). (c) The real (thicker lines) and imaginary (thinner lines) parts of the $|0\rangle$ (solid line) and $|1\rangle$ (dashed line) coefficients.

A sample calculation, shown in Fig. 2.2, depicts the time evolution of the population in each state over the course of their interaction with the laser fields. As expected from the temporal profile of the pulses, the system evolves adiabatically, transferring 100% of the population from $|0\rangle \rightarrow |1\rangle$. Throughout the process the intermediate level $|I\rangle$ never becomes significantly occupied. As a result, no losses are experienced due to spontaneous emission from that state. Seen in Fig. 2.2, which shows the behavior of the $|0\rangle$ and $|1\rangle$ state coefficients, is the additional $\exp(i\pi)$ phase acquired by the final state over the adiabatic passage, this is in agreement with the form of the null eigenvalue in the rotating-wave picture. Up to now the phases of the Stokes and pump lasers fields $\phi_{(S,P)}(t)$ have been set to zero, however by selecting the appropriate relative phase $\chi(t) = \phi_P(t) - \phi_S(t)$, it is possible to control exactly the relative phase given to the target state. If we include these phases and now write the STIRAP Hamiltonian in the interaction representation, solving for the null adiabatic state assuming RWA and the two-photon resonance condition gives us [55]

$$|\lambda_0'(t)\rangle = \cos\vartheta(t)e^{-iE_0t}|0\rangle - e^{i\chi(t)}\sin\vartheta(t)e^{-iE_1t}|1\rangle, \tag{2.32}$$

where E_i for $i = \{0, 1\}$ are the energies of the bare states. Hence by closely monitoring the dynamical phases of each state and by tailoring the relative phases of the pulses, we can obtain precisely the state transfer that is desired.

2.1.4 Comments on APT

The efficiency and versatility of APT methods have been demonstrated in numerous experiments [4, 55, 72]. Its inherent robustness allows for a broad range of schemes to be developed with large scale applicability. The following chapter will demonstrate how the power of adiabatic passage can be harnessed to perform operations that are useful for quantum computations. A review of quantum computing will be given in the next section along with the necessary efficiencies for given operations.

However, as in any adiabatic process the limiting factor in APT is the rate at which the

operations can be carried-out. In optical situations, this means that the laser field must be sufficiently intense over an appreciable amount of time. For certain applications, i.e. those using multi-photon transitions or femtosecond pulses, an APT becomes unfeasible. Often in these cases the necessary laser intensity needed for the system to remain in the adiabatic regime is on the order of the atomic or molecular dissociation energy. As a result a more realistic option become that of femtosecond coherent control [55, 74]. In Chapter 4 we explore an entirely new AP scheme which takes advantage of the additional range of applicability of coherent control techniques while avoiding its well-known short-comings involving the extreme sensitivity to pulse parameters.

2.2 Quantum Computation

2.2.1 Qubits

The fundamental unit used in classical computation and information theory is the *bit* which exists in one of two available states, 0 or 1. Through manipulating a series of bits using basis operations and two-bit interactions any desired algorithm can, in theory, be performed. However occasionally, the algorithm for a particular problem needs an exponential amount of resources (i.e. bits, time) to find a solution, in relation to the dimensions of the problem. In some of these cases computing the solution using a classical computer becomes realistically impossible [38]. In the last decade it was proven that a computer based on manipulating quantum information would be capable of solving a range of such problem more efficiently than a classical system (e.g. simulations of complex quantum systems and prime factoring of large numbers). For this reason an enormous amount of effort has been put forth into developing computer systems based on the principles of quantum mechanics. The quantum analogue to the classical bit, known as a *qubit*, has two possible states $|0\rangle$ or $|1\rangle$, furthermore the qubit may also reside in a superposition of the two states:

$$|\Psi\rangle = \alpha|0\rangle + \beta|1\rangle \ , \tag{2.33}$$

where the complex numbers α and β are normalized such that $|\alpha|^2 + |\beta|^2 = 1$. These two states form the computational basis or orthonormal basis of the Hilbert space and therefore a measurement of the qubit yields state $|0\rangle$ (or $|1\rangle$) with probabilities $|\alpha|^2$ (or $|\beta|^2$). A useful way of representing the state of a qubit is to rewrite Eq. (2.33) as

$$|\Psi\rangle = \cos\frac{\theta}{2}|0\rangle + e^{i\phi}\sin\frac{\theta}{2}|1\rangle \ , \tag{2.34}$$

where θ and ϕ are real numbers. In this representation the possible states of a qubit can be geometrically pictured as the points on the surface of a unit 2-sphere, often called the *Bloch sphere*, where the numbers θ and ϕ define the angles depicted in Fig. 2.2. Since the

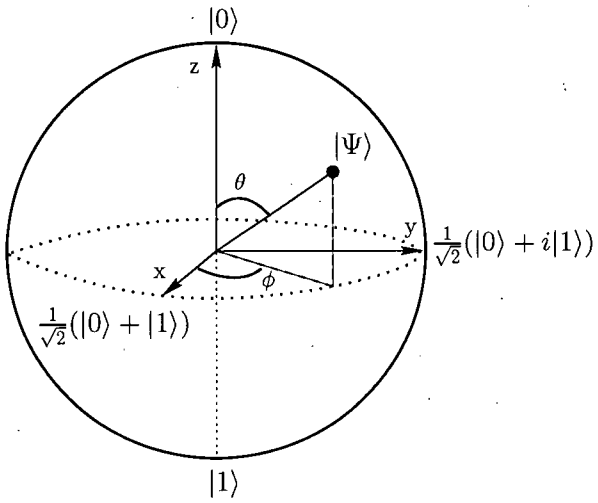

Figure 2.2: Bloch sphere representation of a qubit vector Ψ.

imaginary part of the $|0\rangle$ state can always be turned into a global phase carried by the overall wavefunction $|\Psi\rangle$, this can in turn be ignored because in a single qubit system it would have no observable consequences. This picture becomes useful when considering operations on a single qubit, which can now be viewed as rotations and/or reflections about axes on the Bloch sphere.

A two qubit system, similar to the single qubit, is written as a superposition of its computational basis states. Since each of the two qubits has two possible state, the state vector describing two qubits is

$$|\Psi\rangle_2 = \alpha_{00}|00\rangle + \alpha_{01}|01\rangle + \alpha_{10}|10\rangle + \alpha_{11}|11\rangle, \tag{2.35}$$

where α_{ij} for $\{i,j\} = \{0,1\}$, are the complex coefficients or amplitudes normalized to unity. Notationally, we will count the qubits from left to right, the left-most being the *first* qubit. i.e. the probability of measuring the first qubit in state $|1\rangle$ and the second qubit in state $|0\rangle$ is $|\alpha_{10}|^2$. Note that unfortunately, there is no convenient extension to represent multiple qubit systems, in which any large scale quantum information process could be described. If it is not possible to represent $|\Psi\rangle_2$ as a direct product of the two single qubit states, say ψ_1

and ψ_2, as given in Eq.(2.33),i.e.

$$|\Psi\rangle_2 = (\alpha_1|0\rangle_1 + \beta_1|1\rangle_1) \otimes (\alpha_2|0\rangle_2 + \beta_2|1\rangle_2) \quad (2.36)$$

$$= |\psi_1\rangle \otimes |\psi_2\rangle \ , \quad (2.37)$$

then it is said the two states are *entangled.* A particular important set of entangled two qubit basis states are known as the *Bell states* $|\beta_{jk}\rangle$, succinctly written as

$$|\beta_{jk}\rangle = \frac{|0k\rangle + (-1)^j|1\bar{k}\rangle}{\sqrt{2}} \ , \quad (2.38)$$

where $i, j \in \{0, 1\}$ and the bar ($^-$) represents addition by 1 modulo 2. These states, which are crucial for several quantum mechanical phenomena such as quantum teleportation and superdense coding, will appear in the subsequent chapter. To imagine the potential computational power available to quantum computers we consider an n-qubit system

$$|\Psi_n\rangle = \sum_{\{j_1,\cdots,j_n\}=0}^{1} \alpha_{j_1\cdots j_n}|j_1\cdots j_n\rangle. \quad (2.39)$$

This general n dimensional form contains 2^n amplitudes representing the specific superposition of the states as opposed to only $2n$ coefficients that would be required to describe the state if it were a tensor product space. Harnessing this non-classical entanglement, together with exploiting quantum interferences between the basis states possible because of the Schrödinger wave equation leads to the advantages of quantum computing.

2.2.2 Quantum Gates

The effect of a Hamiltonian governing the evolution of an initial state $|\Psi\rangle$ to some final state $|\Psi'\rangle$ throught the Schrödinger equation, can be expressed in terms of the action of a single unitary operator U on the initial state,

$$\Psi' = U\Psi \ . \quad (2.40)$$

For an n-qubit system the computational space will be a 2^n dimensional Hilbert space, thus the set of allowable operations on the qubits will be elements of $U(2^n)$, the group of $2^n \times 2^n$ unitary matrices. For large n, and therefore for an enormous Hilbert space, such an operation is realistically very difficult to implement directly for the entire array of qubits simultaneously. Thus for most practical applications it becomes necessary to decompose the unitary matrix U into a finite product of several elementary operations or *gates*, U_j, acting on a smaller(≤ 3) number of qubits,

$$U \cong U_1 \times U_2 \times \cdots . \tag{2.41}$$

It has been shown that any operation U can be expressed exactly as a product of unitary operators which act only on a subspace spanned by the computational basis states [38]. Moreover, any U can be approximated to arbitrary accuracy using a finite set of single-qubit rotations and one two-qubit operation. Any such finite set of operators $\{U_1, U_2, \cdots, U_m\}$, which are capable of reproducing U, are known as *universal gate sets*. However, not all universal gate sets are capable of approximating a unitary transform efficiently (i.e. using a polynomials number of gates), in which case we lose the advantages of performing a quantum computation over a classical one. In fact the majority of unitary operations cannot be approximately efficiently at all [38], see Section 2.2.4 for further details. Furthermore, we encounter that the speed of a computation slows down polynomially as the number of the qubits that the operators U_j act upon decrease. Therefore, it is advantageous not to decompose an operation into more elementary parts if its implementation can be done as efficiently as its constituents. Unfortunately, in the general case, only one and two-qubit gates are feasible to implement accurately for a realistic system, and thus we succumb to using the most elementary of universal gate sets; the standard gate set consists two single-qubit gates, the T-gate and *Hadamard*, and a two-qubit *Controlled-NOT* gate. Note that occasionally a third single qubit gate is added to this set, known as the S-gate, but this can be produced from a product of T-gates. If we rewrite the general one and two qubit states

from Eq. (2.33) and (2.35) in vector notation as shown in Eq. (2.42) the action of these gates on the qubits can be understood from their matrix representations,

$$|\Psi\rangle_1 = \begin{pmatrix} \alpha \\ \beta \end{pmatrix}, \quad \text{and} \quad |\Psi\rangle_2 = \begin{pmatrix} \alpha_{00} \\ \alpha_{01} \\ \alpha_{10} \\ \alpha_{11} \end{pmatrix}. \tag{2.42}$$

T-Gate

The T-gate is a specific type of one-qubit phase gate which has the general matrix representation given by

$$\mathbf{R}(\phi) = \begin{pmatrix} 1 & 0 \\ 0 & e^{i2\phi} \end{pmatrix}. \tag{2.43}$$

The curious factor of two in the exponential is an unfortunate convention originating from the definition of the T-gate, otherwise known as the $\pi/8$-gate, which produced a relative phase of $\pi/4$ between the two qubits by giving phases of $\exp(i \pm \pi/8)$ to opposing states. Here the operator $R(\phi)$ acts on the initial state $|\Psi\rangle_1$ of Eq.(2.42) by adding a phase 2ϕ only to state $|1\rangle$, leading to the output state

$$|\Psi_f\rangle_1 = \alpha|0\rangle + e^{i\phi}\beta|1\rangle. \tag{2.44}$$

In the case of the T-gate the phase ϕ equals $\pi/4$. This corresponds to a counter-clockwise rotation of the state vector about the $\hat{z}$ axis in the Bloch sphere representation, see Fig. 2.2. In the discussion of the Hadamard gate we will generalize these rotations of vectors on the Bloch sphere.

Hadamard Gate

One of the most important quantum gates, commonly used to initialize entanglement within a qubit system, is the Hadamard gate represented by the matrix

$$\mathbf{H} = \frac{1}{\sqrt{2}} \begin{pmatrix} 1 & 1 \\ 1 & -1 \end{pmatrix} . \tag{2.45}$$

The action of $\mathbf{H}$ on the initial state $|\Psi\rangle_1$ yields

$$|\Psi_f\rangle_1 = \frac{1}{\sqrt{2}} \Big[(\alpha + \beta)|0\rangle + (\alpha - \beta)|1\rangle \Big] . \tag{2.46}$$

If the qubit was initialized to its ground state $|0\rangle$, as would be likely in a realistic qubit system, then the Hadamard gates would take the qubit into the coherent superposition state $(|0\rangle + |1\rangle)/\sqrt{2}$. In the Bloch sphere picture the Hadamard operation is a $\pi/2$ rotation of the sphere about the $\hat{y}$ axis, followed by a rotation about the $\hat{x}$ axis by π. As is the case for all single qubit gates, this operation can also be expressed as a single rotation by an angle ζ about a particular axis $\hat{n}$ in the Bloch sphere, up to a global phase. Here the general rotation operator $\mathbf{R}_{\hat{n}}(\zeta)$ is defined as

$$\mathbf{R}_{\hat{n}}(\zeta) = \begin{pmatrix} \cos\frac{\zeta}{2} - i\cos\theta\sin\frac{\zeta}{2} & -i\sin\theta\sin\frac{\zeta}{2}e^{-i\phi} \\ -i\sin\theta\sin\frac{\zeta}{2}e^{i\phi} & \cos\frac{\zeta}{2} + i\cos\theta\sin\frac{\zeta}{2} \end{pmatrix} , \tag{2.47}$$

where the unit vector

$$\hat{n} = (\sin\theta\cos\phi, \sin\theta\sin\phi, \cos\theta) , \tag{2.48}$$

in which the angles θ and ϕ are given by those shown in Fig. 2.2. A calculations shows that for the values

$$\zeta = \pi, \qquad \theta = \frac{\pi}{2}, \qquad \phi = 0, \tag{2.49}$$

the rotation in Eq. (2.47) generates the Hadamard gate except for an extra global phase of $\exp(-i\pi/2)$. Taking into account the additional global phase acquired over the rotation the Hadamard gate can be expressed as

$$\mathbf{H} = e^{-i\pi/2}\mathbf{R}_{\hat{n}=\frac{1}{\sqrt{2}}(1,0,1)}(\pi). \tag{2.50}$$

For an isolated qubit this overall phase is unimportant. But if the qubit is part of a larger system of qubits that form a quantum computer, this phase becomes relevant and must be taken into account when performing qubit interactions.

Controlled-NOT Gate

Controlled gates are the most useful operations in classical and quantum computing [38]. These functions will perform a given operation on one or a several *target* qubit if and only if the state of certain *control* qubits is of particular value. In quantum computation the prototypical controlled operation is the 2-qubit controlled-NOT (CNOT) gate. In Table 2.2 the input-output states are shown for the CNOT gate; if the first (control) qubit is set to $|1\rangle$ then the state of the second (target) qubit is flipped, otherwise it is left untouched. The matrix form of the CNOT gate acting on the 2-qubit state in Eq. (2.42),which can be

Quantum State	
In	Out
$\|00\rangle$	$\|00\rangle$
$\|01\rangle$	$\|01\rangle$
$\|10\rangle$	$\|11\rangle$
$\|11\rangle$	$\|10\rangle$

Table 2.2: Input-output table for quantum CNOT gate. The value of the target qubit, given on the right hand-side in the two-qubit ket notation, will be flipped only if the value of the control qubit is 1.

deduced from the truth table, is represented as

$$CNOT = \begin{pmatrix} 1 & 0 & 0 & 0 \\ 0 & 1 & 0 & 0 \\ 0 & 0 & 0 & 1 \\ 0 & 0 & 1 & 0 \end{pmatrix}. \tag{2.51}$$

Thus the initial state $|\Psi\rangle_2$ is transformed into

$$|\Psi_f\rangle_2 = \alpha_{00}|00\rangle + \alpha_{01}|01\rangle + \alpha_{11}|10\rangle + \alpha_{10}|11\rangle. \tag{2.52}$$

2.2.3 Additional Gates

Using the three gates described above any other gate operation can be generated to a specified degree of accuracy. However, there are some cases in which it would be more efficient to implement the desired operation directly instead of decomposing it into a series of these elementary gates from the universal gate set. The following operations are often encountered in quantum algorithm (see Section 2.2.4) and thus are useful to be able to implement directly: controlled-phase gate, SWAP gate, Tofolli gate and the Fredkin gate.

Similar to the CNOT gate, the controlled-phase gate uses a control qubit to determine whether an action will be performed on the target qubit. Under this operation the $|1\rangle$ state of the target qubit will acquire a phase if and only if the state of the control qubit is $|1\rangle$. Traditionally, the phase is equal to $\exp(i\pi/2) = i$ (S-gate), but an arbitrary controlled-phase gate can be defined by

$$X = \begin{pmatrix} 1 & 0 & 0 & 0 \\ 0 & 1 & 0 & 0 \\ 0 & 0 & 1 & 0 \\ 0 & 0 & 0 & e^{i2\phi} \end{pmatrix}, \tag{2.53}$$

where, to be consistent with the earlier definition of the T-gate, 2ϕ represents the value of the additional phase. Generally, the accuracy of implementing a phase related gate is not a

function of the selected phase, as will be seen in Chapter 3, therefore arbitrary phase-gates are useful to incorporate into an algorithm.

The SWAP gate operation, which appears often in quantum algorithms acts on a two-qubit system by swapping the states $|01\rangle \leftrightarrow |10\rangle$. This takes the initial two-qubit state to the output state

$$|\psi_f\rangle_2 = \alpha_{00}|00\rangle + \alpha_{10}|01\rangle + \alpha_{01}|10\rangle + \alpha_{11}|11\rangle. \tag{2.54}$$

A small calculation shows that the SWAP gate can be replicated by three applications of the CNOT gate acting on alternating qubits [3]. Since there is no control component to the SWAP operation it is often easier to implement than CNOT and uses a third of the resources.

Lastly, we quickly mention two three-qubit gates which occasionally make an appearance, these are the Toffoli and the Fredkin gates. The Toffoli, also known as the Controlled-CNOT, gate does as its named suggests, a NOT operation on the target qubit if and only if the *two* control qubits are in state $|1\rangle$. The Fredkin gate, also called the controlled-swap gate, performs a swap operation given the appropriate state of the control bit.

2.2.4 Algorithms

Nearly all general quantum algorithms can be grouped into two classes, those that utilize the quantum Fourier transform (QFT) and those that use a version of Grover's search algorithm. Since this thesis is not directly concerned with the algorithms or their implementations we only give a brief mention of their capabilities. The difficultly in finding other quantum algorithms, or at least ones that would outperform classical methods, lies in the fact that most unitary operations can only be implemented very inefficiently (i.e. require an exponential number of elementary gates from some universal gate set) [38]. As quantum logic operations are decomposed into more and more elementary gates, to ease implementation, a greater and greater number of gate operations are required to accurately approximate the desired unitary transform. Often the overall algorithm cannot be done in polynomial time, even if

the depth of decomposition is lessened to allow for multi-qubit gates due to the additional time cost of implementation. Another limiting factor is the number of times a quantum algorithm must be repeated before a reliable solution is found. If the procedure is not design appropriately, the probabilistic nature inherent in the end measurement of the system may lead to incorrect results, and a number of iterations must be performed to reliably determine the answer.

The algorithms that use the QFT are part of a general Hidden Subgroup problem, of which the notorious Shor's algorithm is a particular case. The order-finding method developed by Shor [58] drew enormous excitement because of its application to prime number factorization, which has a direct relation to the field of cryptography. Relative to all known classical methods, solutions to the factoring problem can be found exponentially faster using the principles of quantum mechanics.

The second major algorithm, nearly entirely developed by Grover [26], can be applied to a variety of search procedures, the most common of which being the search through an unstructured database, where in most cases a polynomial speed-up is seen. See Ref. [19] for a discussion about algorithms using Grover's search.

There exist at least two other categories of quantum algorithms that provide a speed-up over classical methods. Both of these operate in a very case specific manner depending on the computation at hand. The first uses the intrinsic nature of the quantum computing platform to speed-up simulations of quantum systems. Suppose we are interested in the evolution of the initial state of a quantum system, $|\psi(0)\rangle$, under some Hamiltonian, H. After some time t, we wish to know the final state $|\psi(t)\rangle = e^{-iHt}|\psi(0)\rangle$. Now if H can be broken down into a sum of polynomially many terms H_k such that each H_k can be efficiently constructed with a quantum circuit, then a quantum computer can efficiently simulate the evolution e^{-iHt} and obtain an approximation of the final state $|\psi(t)\rangle$. This possibility of performing large scale simulations of systems governed by Schrödinger's equation is perhaps the most intriguing applicability of quantum computing for many scientific researchers. The final class of algorithms, know as adiabatic quantum algorithms, uses a completely different

quantum computing methodology. We note here that this method is not to be confused with proceedings in the following chapter. Otherwise known as adiabatic quantum computations, this route does not involve an individual gate operation. Instead, the system is initiated into the ground state of some Hamiltonian, H_0, upon which a 'problem' Hamiltonian, H_p, is adiabatically turned-on. The total Hamiltonian $H(t)$ can be written as $H(t) = tH_0 + (1 - t)H_p$, where the time, t, is parameterized to flow from $0 \rightarrow 1$. Under adiabatic evolution the state of the system will go from the ground eigenstate of H_0 to the ground eigenstate of H_p, which holds the solution to the problem. Although several NP-complete problems may be solvable using this methodology, this is aside from this thesis discussion and such not be confused with the ideas of implementing individual gates using an adiabatic evolution.

2.2.5 Fault-Tolerance

It is important to consider the effects of errors that arise from either imperfect implementation of quantum logical operations or uncontrolled interaction of the system with the environment, to the processing of quantum information. If the errors in approximating a particular unitary operation on a system of qubits become too large then the output becomes meaningless and we fail to find the solution to the problem at hand. Realistically, every operation carried-out on a quantum system can only be implemented with some non-perfect efficiency [44], thus it is necessary to enstate some form of quantum error correction such that the inevitablely arising errors can be controlled and do not become amplified by propagating throughout the remainer of the quantum curcuit. If a system continues to operate reliably, even once the performance of its subsystems (ie. fidelity of the gate operations) fall to some non-perfect level of accuracy, then we call such a design *fault-tolerant.* It was found that the deleterious effects of decoherence in a quantum computation could be avoided if the average probability of error per quantum gate is less than a certain critical value [23, 57]. This critical value, also known as the *fault-tolerant threshold*, is typically taken to be 10^{-4}. Once this occurs, quantum error-correcting codes and fault-tolerant procedures can be incorporated into the circuit design to enable us to perform arbitrarily long

quantum computations with arbitrarily high reliability, even if occasional mistakes occur during the error-recovery process; although several groups ([33, 60]) have now relaxed the necessary fidelity rates of quantum gates to lie between the values of 99.9% and 99.99% .

2.2.6 Physical Realizations

There are several platforms under consideration for quantum computation each with different possible methods for implementing logic operations. Table 2.3 ([6]) shows a summary of several approaches currently under study, different from that discussed in the following section. The curious reader can refer to reference [38] for more details.

	Quantum Computing Systems						
	NMR	Solid State		Linear Optical	Quantum Optical		
					Trapped Ion	Flying Atom	
						μwave	Optical
Qubits	Nuclear Spins	Quantum Dots	Cooper Pairs	Photon	Trapped Ions	Flying Atoms	Flying Atoms
Qubit Control	Magnetic field	Tunnel junction	Magnetic field, Electrostatic gates	Beam splitters	Kerr medium	Laser pulses	μ-wave
Interaction	Zeeman J-coupling	Heisenberg coupling	Josephson junctions	Jaynes-Cummings (JC)	JC	JC	JC
Interaction time	1 μs-1 ms	10^{-13}s	100 ps	-	1 ms	10-100 μs	1 μs
Decoherence time	10^{-2}-10^{8}s	100 fs - 100 ps	1 μs	-	10^{-1}s	1 ms	10^{-5}s
Decoherence source	Spin relaxation	Distant charge motion	Spontaneous emmission	-	Phonon decay	Cavity decay	Cavity debay

Table 2.3: Summary of several current quantum computing platforms. The type of system and implementation method is shown along with some physical properties [38].

Chapter 3

Computation using Adiabatic Passage between Molecular Levels

3.1 Introduction

There have been many proposals of implementing universal gate-sets on various quantum systems [38], some of which were outlined in the previous chapter. In the past few years, a number of authors have also considered using the vibrational modes of molecules as platforms for quantum computations. Most of these papers[2, 40–42, 65, 68, 69] have derived the pulses that produce the desired logic gate numerically, using Optimal Control Theory (OCT)[48, 56, 64]. The drawback of this approach is that the pulses thus produced are critically dependent on the exact knowledge of the potential energy surface(s) on which the nuclei move. Such knowledge is usually not accurate enough for high fidelity operations. In addition, the pulses obtained using OCT are extremely sensitive to the pulse details. For example, like in the use of a π-pulse to induce population exchange between two levels, the OCT derived pulses are extremely sensitive to the *pulse area*. Moreover, the OCT derived pulses are sensitive to the exact *phase chirp* and *pulse shape*. Since in real experiments it is very difficult to produce pulses whose parameters are accurate to within a fraction of a percent, as dictated by the quantum computation requirements, the method is very difficult, if not impossible, to apply in practice.

Adiabatic turn-on and turn-off of an interaction appears to be a natural direction for performing operations needed for quantum computation. Recently, several groups have proceeded in this general direction and have suggested using alternate methods such as

"Adiabatic Quantum Computing" [10, 18, 24, 31, 52, 61] and "Holonomic Computing" [36, 46, 76, 79], for performing logic manipulations in various systems.

Here we take a seemingly easier adiabatic approach, relying on Adiabatic Population Transfer (APT) between sets of three and four quantum levels. The main idea is to build *all* the gates required for a universal gate set via the in-tandem applications of Adiabatic Passage (AP) [5, 20, 22, 32, 50, 51] steps.

In contrast to the numerically derived OCT-based pulses, APT is very robust. Once the theoretically specified order of delay times and *adiabatic conditions* $\Omega_i\tau_i \gg 1$, where Ω_i is an effective Rabi frequency of the i^{th} pulse, and τ_i is its duration, are met, APT is rather insensitive to the exact values of Ω_i and τ_i and other pulse parameters [5, 20, 55, 73]. However, in our case, since we will be using a non-degenerate encoding for the qubits, the duration τ for each pulse will have to be precisely defined such that the optical phase accumulations of the states can be included into our scheme. With the pulse duration specified, this will still allow for significant variations in the pulse intensities dictated by the adiabatic conditions. Moreover, because APT is a generic scheme it does not change in essence from one set of levels to another. In this application, it involves resonant transitions between a small (3 or 4) number of levels, the input for the universal gate set construction consists of a few dipole matrix elements, which, if necessary, can be measured experimentally. No theoretical knowledge of an entire potential energy surface is necessary.

The APT based logic gates we demonstrate rely mainly on introducing the pulses in the right sequence and maintaining the electric field's amplitudes and its analytically-derived phases in accordance with the requirements of the logic operation at hand. Below we demonstrate both the great stability and the near-perfect gate fidelities one can achieve in the one- and two-qubit Na_2 systems. Because of the universality, this method can be implemented in other quantum gates not explicitly considered here and is scalable to larger multi-(≥ 3)-qubit systems [22].

3.2 Sodium Molecule

3.2.1 Numerical Calculations

Due to its presence in our lab, and also, to the availability of a large amount of experimental data [9, 11, 30, 53], the sodium molecule is a convenient platform to test our logic gates. Necessary for our simulation, we calculated the eigenstates and their corresponding energies for various potential energy surfaces of the Na_2 dimer, along with the required Franck-Condon (FC) factors for the expected transitions. To determine the form of the electronic manifolds, the energy was obtained at various points along the potential curve using ab initio calculated data from Ref. [53]. The data is given for 20 internuclear distances, for two different potential surfaces in Table 3.1; additional data points were obtained using a cubic spline interpolation routine [45].

Internuclear Distance	Energies	
	$X^1\Sigma_g^+$	$B^1\Pi_u$
3.75	0.01981	0.124806
4.0	0.0063	0.110423
4.5	-0.011977	0.089841
5.0	-0.022046	0.076887
5.5	-0.026403	0.06947
6.0	-0.026949	0.065991
6.5	-0.025152	0.065149
7.0	-0.02209	0.065948
7.5	-0.018515	0.067646
8.0	-0.014935	0.069721
8.5	-0.011663	0.071817
9.0	-0.008863	0.073712
10.0	-0.004812	0.076499
11.0	-0.002493	0.077968
12.0	-0.001279	0.078538
13.5	-0.000489	0.078604
15.0	-0.000205	0.078357
17.0	-7.6^{-5}	0.077998
20.0	-2.2^{-5}	0.077606
30.0	-2.0^{-6}	0.077096

Table 3.1: Data taken from Ref. [53] for the energies of two potential energy surfaces in Na_2 as a function of internuclear distance; all values are listed in atomic units.

Given the potential at a set of discrete points, the eigenvalues and eigenstates were found using a finite difference algorithm. All calculated energies were found to be within 0.1% of previous theoretical and experimental values cited in Ref. [9]. The FC factors between levels were determined by calculating the overlap between eigenstates using numerical integration methods. The values used for our simulations are shown in Tables 3.2 and 3.3.

3.2.2 Structure and Encoding

Consider a single qubit in an arbitrary state given by

$$|\Psi_i\rangle = \alpha|0\rangle + \beta|1\rangle \tag{3.1}$$

which has the typical normalization such that $|\alpha|^2 + |\beta|^2 = 1$. In performing the APT scheme, two additional non-degenerate states are introduced, as shown in Fig. 3.1. The first additional state, labeled $|S\rangle$, is used for temporary population shelving. It must therefore be long-lived relative to the duration of the gate operation. This is not a very restrictive requirement because our pulse durations will be in the ps-ns domain. The second additional state, labeled $|I\rangle$, acts as the intermediate state in the APT population transfer scheme. Because it never gets populated, its actual lifetime is of no importance. In the APT scheme, we use as the intermediate state, that must be coupled to the two other levels, a ro-vibrational state belonging to an electronic manifold different than that of the initial/final states. In this way we minimize the restrictions imposed by the optical selection rules. For example, transitions within the same electronic state depend upon the presence of a permanent electric dipole moment which is absent for homonuclear diatomics and is confining for heteronuclear diatomics; levels couple to a given state by the $\Delta J = \pm 1$ and $\Delta v \approx \pm 1$ selection rules, where v and J label the vibrational and rotational quantum numbers, respectively [29]. More specifically, we select low-energy ro-vibrational levels, $|v, J\rangle$, in the $B^1\Pi_u$ electronic state of Na_2 to house our intermediate levels. These states are optically accessible from nearly all of the $X^1\Sigma_g^+$ ground states, and have transition dipole moments, $B \rightarrow X$,

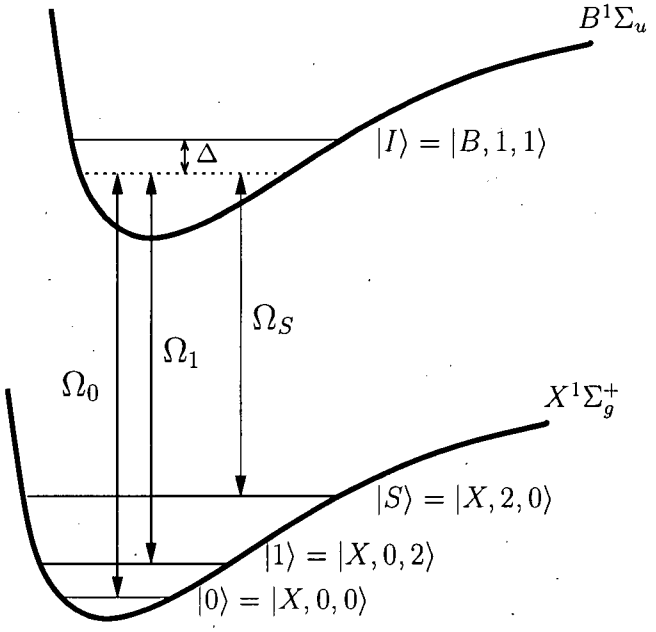

Figure 3.1: One-qubit interaction scheme depicted between the rovibrational eigenstates of two potential energy surfaces in Na_2. The states are labeled as $|a,i,j\rangle$ where a represents the electronic state, then i and j the vibrational and rotational levels repectively.

that are less dependent on internuclear distance than other electronic surfaces (e.g., $A^1\Sigma_u^+$) [62].

Because both the shelving state and the states used to store the qubits ("qubit states") should be stable against decoherence due to spontaneous emission, we use low-lying ro-vibrational eigenstates in the ground electronic state, $X^1\Sigma_g^+$, of the Na_2 molecule. The average life-time of these states may be as long as a few milliseconds (ms) [35], allowing plenty of time for the completion of all logic operations of interest.

We have chosen to use a diatomic molecule so as to avoid an additional coupling between qubit states and non-qubit states belonging to other vibrational modes of the same molecule, a complication encountered by other groups using polyatomic molecular states coupled by broad band pulses. [68].

3.3 Implementation

The general scheme for implementing the various gate operations on our molecular system relies on the consecutive application of two APT processes. The arbitrary-phase and controlled-not gates will use a double application of the STIRAP procedure discussed in Section 2.1.3. For the Hadamard operation the basic STIRAP scheme will be replaced by a modified version involving four levels. This new scheme is presented in the corresponding section. An important prerequisite for the success of any adiabatic scheme is that each of the states be individually addressable by the laser pulses. This means that each Rabi frequency involved must couple only one of the degenerate states to the excited 'transfer' state. Additionally, any of the excited levels involved in the procedure must be sufficiently long-lived to eliminate the loss of coherence via decay.

In the present application, the anharmonicity of the electronic potential energy surface of the molecule is sufficient to guarantee the one-to-one correspondence between the laser frequencies and the transition frequencies, resulting in easy and accurate addressability. Considering that the typical spacings between two low-lying ro-vibrational eigenstates is

~ 0.001 eV, our gate operations can be done using lasers with as short as picosecond (ps) pulses. However, because we are dealing with various excited levels attention must be paid to the spontaneous decay rates and to the effect of each state's different dynamical phase evolution when we perform the procedures. As the gate simulations show, the relatively slow decay from the participating states is negligible when compared to the duration of the operation. The pulse time scales are much shorter than the recorded average lifetimes of excited ro-vibrational levels in the ground state electronic surface [35], allowing us to completely avoid decoherences due to spontaneous decay.

3.3.1 Numerical Simulations

The viability of the following schemes are demonstrated by performing a number of simulations of one- and two-qubit systems encoded in Na_2 molecule. In all cases our simulations are derived from a numerical solution of the Schrödinger equation using a molecular set of energy levels, coupled through electric-dipole matrix elements by pulses satisfying the adiabatic condition. We present our results in the interaction representation, thus omitting the dynamical phase of each of the states from the figures. These phases can each be monitored and integrated into these schemes by the appropriate timing and durations of the laser pulses. In addition to establishing the very high fidelity rates of our schemes, our simulations also serve to obtain realistic estimates for the durations of the various gate operations. For all cases studied we have conservatively considered laser powers of approximately 10 MW/cm^2 and pulse durations of 100 ps, which satisfy the adiabatic conditions for most optically-allowed molecular transitions.

The fidelity of each gate is computed as the overlap between the expected wave function, $|\Psi\rangle$, and that obtained numerically, $|\psi_n\rangle$, at the conclusion of each gate operation. We show that the fidelities for the $\pi/8$-phase (T), Hadamard and CNOT gates, which make-up a universal and fault-tolerant basis for quantum computation [7], are all essentially unity. Note that, these gates comprise the 'standard' 4-element universal gate-set: The π-phase shifter (S), T, Hadamard and CNOT gates. Since S is related to T it suffices to demonstrate

the implementation of T.

3.3.2 One-qubit Gates

For the single qubit operations we take the $v = 1, J = 1$ state in $B^1\Pi_u$, $|B, 1, 1\rangle$, as our intermediate level. By the optical selection rules we know that this will couple strongly to at least the three ro-vibrational levels in $X^1\Sigma_g^+$, $|X, v = 0, J = 0\rangle$,$|X, v = 0, J = 2\rangle$, and $|X, v = 2, J = 0\rangle$ which we use to represent the $|0\rangle$, $|S\rangle$, and $|1\rangle$ states respectively. This restrictive coupling between eigenstates allows us to avoid decoherence during our gate operations due to off-resonant couplings between other non-participating states. The relevant Franck-Condon factors are calculated using a discrete-variable representation method which has been validated using previously published calculations [9, 11]. The energies of the involved states and their corresponding FC factors to the intermediate level are shown in Table 3.2. The energies are scaled relative to the value of the dissociation energy of 6022.03 cm^{-1} of the ground electronic state [30].

State	Quantum #	Energy(a.u.)	FC factor
$\|0\rangle$	$\|X, 0, 0\rangle$	-0.0267275	0.2638
$\|1\rangle$	$\|X, 2, 0\rangle$	-0.0253013	0.5219
$\|S\rangle$	$\|X, 0, 2\rangle$	-0.0267229	0.2640
$\|I\rangle$	$\|B, 1, 1\rangle$	0.0654244	X

Table 3.2: Energies and FC factors in Na_2 for the one-qubit gate simulations.

Arbitrary Phase Gate

The effect of the phase gate discussed in Sec. 2.2.2 on a single qubit state, Eq. (3.1), is the addition of a relative phase ϕ to the phase of state $|1\rangle$ while leaving the state $|0\rangle$ untouched. The fact that a population transfer between two states using the STIRAP method adds a controllable phase to the final state leads to an obvious implementation of the phase gate operation. That is, by the consecutive application of two adiabatic passages involving the shelving state $|S\rangle$. In the first step two laser pulses with real Rabi frequencies $\Omega_1(t)$ and

$\Omega_S(t)$ (see Fig. 3.1), tuned to be in resonance with the $|1\rangle - |I\rangle$ and $|I\rangle - |S\rangle$ transitions, respectively, are used to adiabatically transfer the entire population of state $|1\rangle$ to state $|S\rangle$. In the second step, the population is transferred back from state $|S\rangle$ to state $|1\rangle$, however this time we use a complex Rabi frequency $\Omega_S(t) = |\Omega_S(t)|e^{i\phi}$. The second pulse sequence induces the $|S\rangle \rightarrow e^{i\phi}|I\rangle \rightarrow e^{i\phi}|1\rangle$ two-photon process. The net result of both steps is to encode a phase ϕ onto state $|1\rangle$ exclusively. The complete success of this strategy is demonstrated below.

$\pi/8$-phase gate operation

Initializing our system to be the $|+\rangle$ one-qubit state,

$$|\Psi_i\rangle = |+\rangle = \frac{1}{\sqrt{2}}(|0\rangle + |1\rangle) \ , \tag{3.2}$$

a T-gate operation adds a relative phase to $|1\rangle$ such that our state goes into

$$|\Psi_f\rangle = \frac{1}{\sqrt{2}}(|0\rangle + (\alpha_+ + i\alpha_-)|1\rangle) \ , \tag{3.3}$$

where $\alpha_\pm = \left(2 \pm 2^{\frac{1}{2}}\right)^{\frac{1}{2}}/2$.

In Fig. 3.2 we present a simulation of this logic gate. As shown in panel (c) the final values obtained numerically are *exactly* the desired values of Eq. (3.3). Thus the gate fidelity is virtually perfect! We see that, as required, the first APT process, which uses the pulse sequence Ω_S and Ω_1, completely transfers the population of state $|1\rangle$ to state $|S\rangle$. When the process is reversed and a $\pi/8$-phase is imparted to Ω_S, the population flows back to the initial state, which acquires exactly a $\pi/8$ phase. It is evident from Fig. 3.3.2 that even with the conjoining of the two pulses between the APTs, gate fidelities in our Na_2 system remain in excess of 99.9 % . The minor reduction in fidelity can be attributed to additional laser couplings between off-resonant levels in our molecule resulting in the temporary occupation of the intermediate level and the minor deviation of the imaginary part of the $|0\rangle$ coefficient

from zero shown in Fig. 3.3.

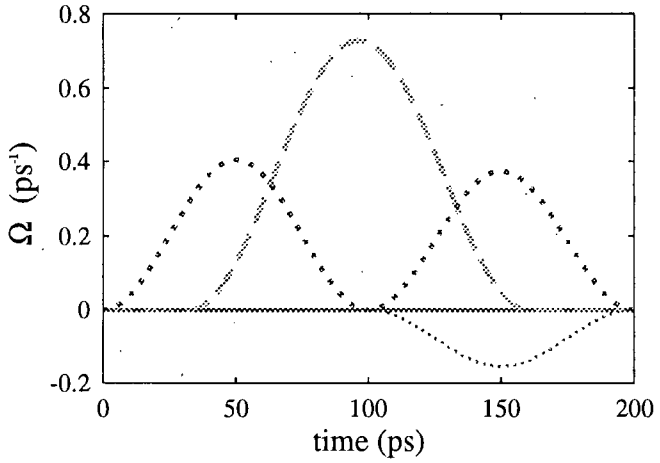

Figure 3.2: (a)

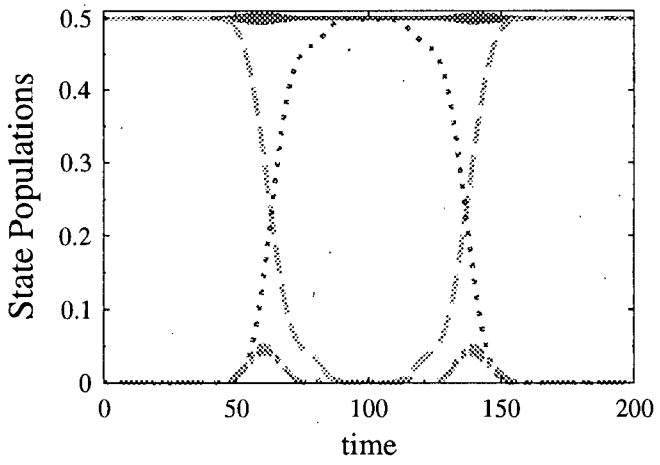

Figure 3.2: (b)

from zero shown in Fig. 3.3.

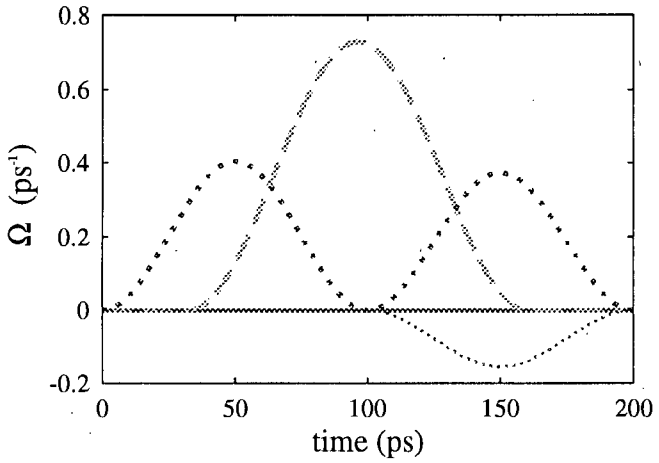

Figure 3.2: (a)

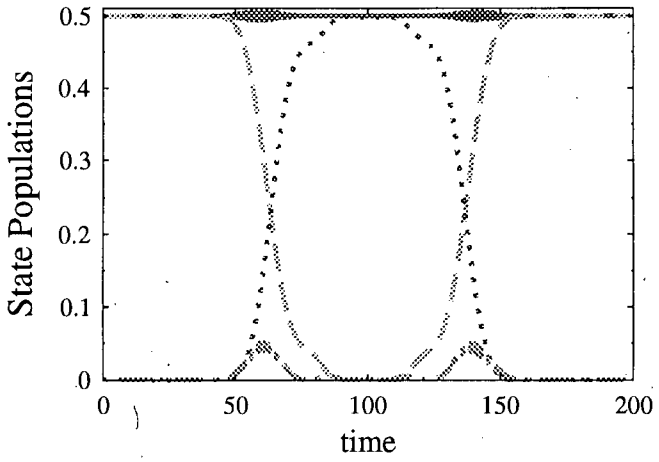

Figure 3.2: (b)

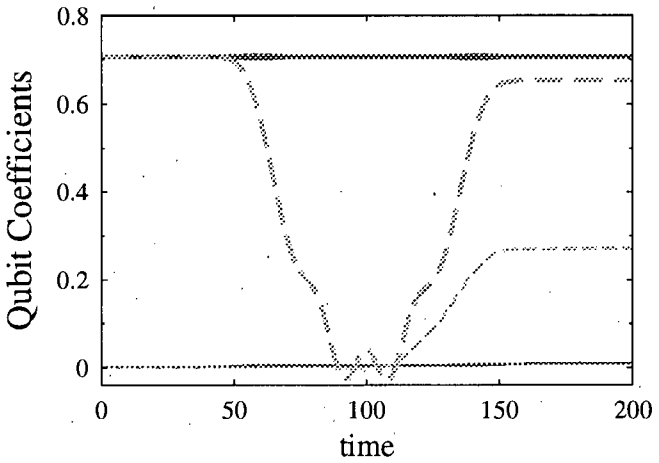

Figure 3.2: (c)

Figure 3.2: Numerical simulation of the $\pi/8$-phase gate implemented on a one-qubit system initialized to an even superposition of the $|0\rangle$ and $|1\rangle$ qubit states. Where present, the thinner lines on the plots represent the imaginary part of the variable corresponding to that line type. All times shown are in picoseconds. (a) Profiles of the Rabi frequencies, Ω_i, for each of the pulses in resonance with the $|i\rangle - |I\rangle$ transitions used to carry-out the gate operation. Solid line: Ω_0. Dashed line: Ω_1. Dotted line: Ω_S. Notice that only the last pulse contains an imaginary part due to the added phase shift. Units are $1/ps$. (b) Temporal evolution of the probability amplitudes for each of the states: $|0\rangle$ (solid line), $|1\rangle$ (dashed line), $|S\rangle$ (dotted line) and $|I\rangle$ (dot-dashed line). As expected the final populations of the $|0\rangle$ and $|I\rangle$ states are not significantly affected. (c) The real and imaginary parts of the qubit coefficients: $|0\rangle$ (solid line) and $|1\rangle$ (dashed line). The thicker upper two lines on the right-hand side of the plot represent the real parts of each state's coefficients.

We note that here, and in nearly all of the following simulations presented below where a chain of elementary APT processes is constructed to yield a complex logical operation, the pulse that terminates one elementary APT process may, in fact, be identical in all aspects to the pulse that initiates the subsequent step. As we show in this example, in such cases we can conjoin these two pulses into one pulse. The use of such conjoined pulse chains simplifies the experimental setup and saves on gate operation times.

Hadamard Gate

The implementation of a Hadamard gate is understandably more complicated than that of a phase gate. Instead of having to manipulate a single rovibrational state of the molecule, the Hadamard gate requires the ability to control simultaneously both of the available qubit states, $|0\rangle$ and $|1\rangle$ in a specific manner. In the last few years a number of papers have studied the adiabatic manipulation of four-states in the so-called 'tripod' system [67, 70], which consists of a threefold degenerate ground state coupled to a single excited state. A similar scheme to that presented in Ref. [32] will be presented here to implement the Hadamard gate in our non-degenerate molecular system. The interaction scheme shown in Fig. 3.1 is identical to that used for the phase gate operations except for the presence of an additional laser field coupling states $|0\rangle$ and $|I\rangle$. For the theoretical discussion, it will be assumed that each of the three laser fields $(\Omega_0, \Omega_1, \Omega_S)$ drives only their respective transitions, as depicted in the figure. Using the same method of implementation as the phase gate, this scheme also uses two consecutive APT sequences. In the first APT process the Ω_S pulse acts as the Stokes field and *both* the Ω_0 and Ω_1 pulses behave as the pump field. The initial population occupying the qubit basis states is taken into a superposition of $|0\rangle$, $|1\rangle$ and $|S\rangle$. In the second step the fields are applied in the reverse order and an extra phase is added to the Ω_S pump pulse. As will be shown, with the appropriate selection of Rabi frequencies in Eq.(3.4) the population is returned to the qubit states in a manner identical to that of a Hadamard operation. Following the analysis used in earlier APT schemes, it will be helpful to study the behavior of the instantaneous eigenstates of the system's Hamiltonian. Similar to the two-photon condition in the traditional STIRAP, the system here is in a multi-photon resonance, therefore the detunings of the three lasers are identical and will be labeled by Δ. To further simplify the algebra, the three pulsed Rabi frequencies will have the same field

envelopes, $\Omega(t)$, and will be characterized as

$$\begin{aligned} \Omega_0(t) &= \Omega(t)\cos\chi \\ \Omega_1(t) &= \Omega(t)e^{i\eta}\sin\chi \\ \Omega_S^{(k)}(t) &= \Omega(t-\tau^{(k)})e^{i\delta^{(k)}} \end{aligned} \tag{3.4}$$

where χ and η are predetermined angles. The superscript ($k = 1, 2$) denotes the k^{th}-AP process, with Stokes-pump pulse delay $\tau^{(k)}$ and relative phase $\delta^{(k)}$ between those pulses. Using the interaction representation, the Hamiltonian of this system is written, omitting the k-superscripts, in the RWA as

$$\mathbf{H}(t) = \frac{1}{2}\begin{pmatrix} 0 & 0 & 0 & \Omega(t)\cos\chi \\ 0 & 0 & 0 & \Omega(t)e^{i\eta}\sin\chi \\ 0 & 0 & 0 & \Omega(t-\tau)e^{i\delta} \\ \Omega^*(t)\cos\chi & \Omega^*(t)e^{-i\eta}\sin\chi & \Omega^*(t-\tau)e^{-i\delta} & 2\Delta \end{pmatrix} . \tag{3.5}$$

where $\{|0\rangle, |1\rangle, |S\rangle, |I\rangle\}$ define the basis states. Diagonalizing the 4x4 Hamiltonian in Eq.(3.5) we calculate the eigenvalues, a_j, and determine their corresponding eigenvectors $|a_j\rangle$ for $j = \{1, 2, 3, 4\}$:

$$\begin{aligned} |a_1 = 0\rangle &= \Omega^*(t-\tau)|0\rangle - \Omega^*(t)e^{i\delta}\cos\chi|S\rangle \ , \\ |a_2 = 0\rangle &= -\sin\chi|0\rangle + e^{i\eta}\cos\chi|1\rangle \ , \\ |a_3 = -\frac{\Lambda(t)}{2}\rangle &= \Omega(t)\cos\chi|0\rangle + \Omega(t)e^{i\eta}\sin\chi|1\rangle + \Omega(t-\tau)e^{i\delta}|S\rangle - \Lambda(t)|I\rangle \ , \\ |a_4 = \frac{\Lambda(t)}{2}\rangle &= \Omega(t)\cos\chi|0\rangle + \Omega(t)e^{i\eta}\sin\chi|1\rangle + \Omega(t-\tau)e^{i\delta}|S\rangle + \Lambda(t)|I\rangle \ , \end{aligned} \tag{3.6}$$

where $\Lambda(t) = \sqrt{|\Omega(t)|^2 + |\Omega(t-\tau)|^2}$. From the above adiabatic states it can be seen that the pump fields ($\Omega_0(t)$ and $\Omega_1(t)$) allows a connection to be made from the bare basis states

$\{|0\rangle, |1\rangle, |S\rangle, |I\rangle\}$ to the basis $\{|c\rangle, |nc\rangle, |S\rangle, |I\rangle\}$, where

$$|c\rangle = \cos\chi|0\rangle + e^{i\eta}\sin\chi|1\rangle \tag{3.7}$$

$$|nc\rangle = |a_2\rangle = -\sin\chi|0\rangle + e^{i\eta}\cos\chi|1\rangle \ . \tag{3.8}$$

are the states that are coupled(c) and non-coupled(nc) to the shelving state $|S\rangle$. If the initial state of the system $|\Psi\rangle$ is now rewritten in the new basis,

$$|\Psi_i\rangle = \langle nc|\psi_i\rangle|nc\rangle + \langle c|\psi_i\rangle|c\rangle \ , \tag{3.9}$$

where $\langle c|\Psi_i\rangle$ and $\langle c|\Psi_i\rangle$ can easily be determined from Eq. (3.1) and (3.7), it becomes apparent that only a fraction of the population in the qubit basis states are affected by the lasers. More specifically, the first APT process with $\tau^{(1)} > 0$ will transfer only the population residing in the coupled state to the shelving state. As in the traditional STIRAP, the intermediate state never becomes occupied. Here this is due to the interference between the two pathways of the two adiabatic states $|a_3\rangle$ and $|a_4\rangle$, which have opposing signs of the $|I\rangle$ component. Thus, after the first pulse sequence the system is left in the following superposition of two states

$$|\psi\rangle = \langle nc|\psi_i\rangle|nc\rangle - e^{i\delta^{(1)}}\langle c|\psi_i\rangle|S\rangle \ . \tag{3.10}$$

This looks strikingly similar to the final state of the original STIRAP transition shown in Eq. (2.32). Here, the transfer occurs between the states $|c\rangle$ and $|S\rangle$, where $\delta^{(1)}$ is the controllable phase. In fact, the Hamiltonian in Eq. (3.5) could have been rewritten using the new basis states $\{|nc\rangle, |c\rangle, |S\rangle, |I\rangle\}$ in the form

$$\mathbf{H}(t) = \frac{1}{2}\begin{pmatrix} 0 & 0 & 0 & 0 \\ 0 & 0 & 0 & \Omega(t) \\ 0 & 0 & 0 & \Omega(t-\tau)e^{i\delta} \\ 0 & \Omega^*(t) & \Omega^*(t-\tau)e^{-i\delta} & 2\Delta \end{pmatrix} , \tag{3.11}$$

which is identical to the Hamiltonian in Eq. (2.27) for an ordinary three-level STIRAP. In the second step the pulses are applied in the reverse order taking the population in the state $|S\rangle$ back to the qubit subspace. Upon initial review this second APT may appear problematic; the two Stokes fields, Ω_0 and Ω_1, are coupling two *populated* states to the intermediate level. In general, the final (or target) state in an APT cannot be occupied, otherwise, when the Stokes field performs the initial coupling it will induce Rabi-like oscillations between the final and intermediate levels. As a result we do not achieve a clean projection of the wave vector onto a single adiabatic state, which in lieu causes population mixing between all levels. Fortunately, with further consideration we notice that the final state of the first APT process, Eq. (3.10), is actually a dark state of the initial laser fields. For one, the state $|S\rangle$ is not initially coupled, and secondly the Stokes fields only affect the $|c\rangle$ component of the qubit basis states and $|\Psi\rangle$ has only a $|nc\rangle$ component orthogonal to the coupled state $|c\rangle$. The second STIRAP will thus map the state $|S\rangle$ back to $|c\rangle$ such that the initial component of $|\Psi_i\rangle$ along $|c\rangle$ will differ from the final component of the same states by only a phase. This phase, δ, results from a difference between the relative phases of the fields (Ω_1, Ω_1) and Ω_S in the two transfer processes. In the adiabatic limit the final state can be written as

$$|\Psi_f\rangle = \langle nc|\Psi_i\rangle|nc\rangle + e^{-i\delta}\langle c|\Psi_i\rangle|c\rangle , \tag{3.12}$$

where $\delta = \delta^{(1)} - \delta^{(2)}$. Rewriting $|\Psi_f\rangle$ in the qubit basis $\{|0\rangle, |1\rangle\}$ we have

$$\begin{aligned} |\Psi_f\rangle = &\left(\alpha\left(\sin^2\chi + e^{-i\delta}\cos^2\chi\right) + \beta e^{-i\eta}\sin\chi\cos\chi\left(e^{-i\delta} - 1\right)\right)|0\rangle \\ &+ \left(\alpha e^{i\eta}\sin\chi\cos\chi\left(e^{-i\delta} - 1\right) + \alpha\left(\cos^2\chi + e^{-i\delta}\sin^2\chi\right)\right)|1\rangle . \end{aligned} \tag{3.13}$$

Simplifying the expression using a few trigonometric identities and writing the final state in terms of an overall evolution matrix acting on the initial qubit vector $(\alpha, \beta)^T$, we obtain

$$|\psi_f\rangle = e^{-i\frac{\delta}{2}} \begin{pmatrix} \cos\frac{\delta}{2} - i\cos 2\chi \sin\frac{\delta}{2} & -i\sin 2\chi \sin\frac{\delta}{2} e^{-i\eta} \\ -i\sin 2\chi \sin\frac{\delta}{2} e^{i\eta} & \cos\frac{\delta}{2} + i\cos 2\chi \sin\frac{\delta}{2} \end{pmatrix} \begin{pmatrix} \alpha \\ \beta \end{pmatrix} . \tag{3.14}$$

We find that the evolution operator for this entire two-step STIRAP procedure is a global phase $\exp(-i\delta/2)$ multiplied by the general rotation operator, $\mathbf{R}_{\hat{n}}(\delta)$, discussed in Section 2.2.2. Recall, this operator describes a single qubit rotation by an angle δ about an axis $\hat{n} = (\sin 2\chi \cos\eta, \sin 2\chi \sin\eta, \cos 2\chi)$. Therefore, by tuning the relative strengths of the fields Ω_0 and Ω_1 and selecting the appropriate relative phases, δ, of the fields any single qubit unitary operation can be performed. In this case we use the previously calculated values shown in Eq. (2.49) to determine the correct field parameters to implement the Hadamard gate. Specifically, these values are found to be

$$\Omega_0(t) = \Omega(t)\cos\frac{\pi}{8} , \qquad \Omega_1(t) = \Omega(t)\sin\frac{\pi}{8} , \tag{3.15}$$

$$\Omega_S^{(k)}(t) = \Omega(t - \tau^{(k)})e^{i\delta^{(k)}} \quad \text{where} \quad \delta^{(1)} - \delta^{(2)} = \pi . \tag{3.16}$$

Hadamard gate operation

In Fig. 3.2 we show the results of simulating the one-qubit Hadamard gate starting from a single initial state ($|0\rangle$), using the Rabi frequencies as described above. As shown in panel (b) of that figure, our initial state evolves into precisely the $|+\rangle$ state of Eq. (3.2). As in the phase gate, changes in the timings between the two APT processes do not reduce the essentially perfect gate fidelity. As illustrated in Fig. 3.2(b), the first APT step takes the system into a superpositions of the $|0\rangle$, $|1\rangle$ and $|S\rangle$ states, in which the shelving state is occupied for approximately 100 ps. The second AP step then completes the transfer.

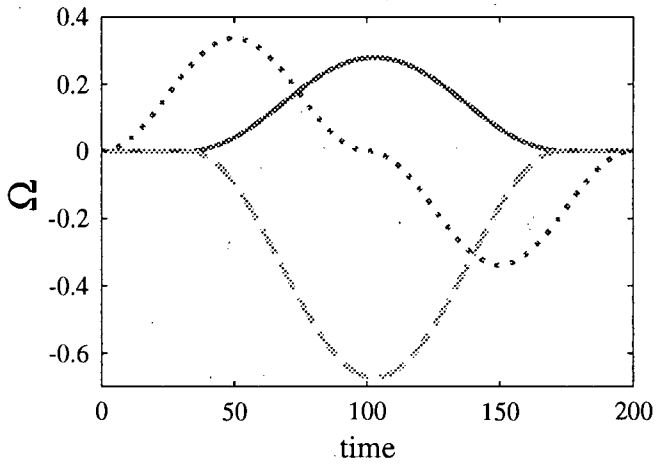

(a)

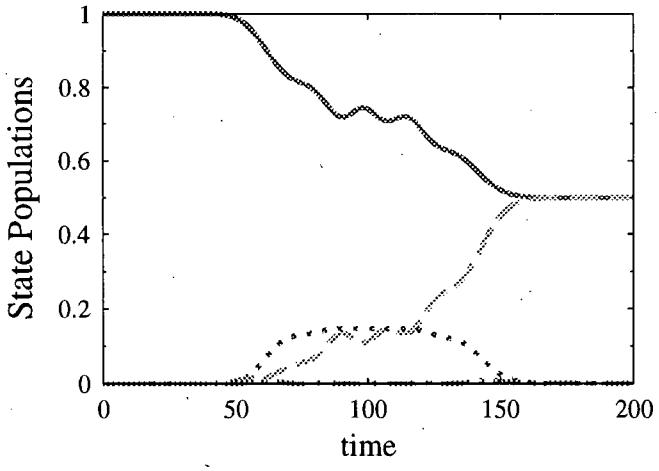

(b)

Figure 3.2: Calculations for the implementation of a Hadamard gate on our one-qubit system beginning in the state $|0\rangle$. Same units as in Fig.3.2. (a) Temporal evolution of the three real valued Rabi frequencies of the pulses coupling each of the states to $|I\rangle$. Solid line: Ω_0. Dashed line: Ω_1. Dotted line: Ω_S. (b) The populations of the four state: $|0\rangle$ (solid line), $|1\rangle$ (dashed line), $|S\rangle$ (dotted line) and $|I\rangle$ (dot-dashed line), throughout the gate operation.

3.3.3 Two-qubit Gates

We now consider an arbitrary two-qubit state given by

$$|\psi\rangle_2 = \alpha_{00}|00\rangle + \alpha_{01}|01\rangle + \alpha_{10}|10\rangle + \alpha_{11}|11\rangle, \tag{3.17}$$

normalized to unity. Similar to the one-qubit case we encode the four qubit states and two additional states, $|I\rangle$ and $|S\rangle$, in six particular ro-vibrational eigenstates of our molecule. As before $|I\rangle$ acts as the intermediate state, used to transfer population to and from the shelving state $|S\rangle$. The desired gate operation determines which states out of the four qubit states get coupled to the $|I\rangle$ state.

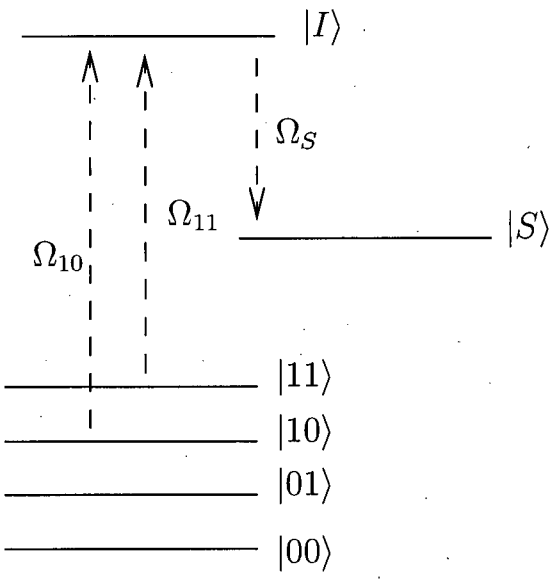

Figure 3.3: Two-qubit interaction scheme for the implementation of the CNOT gate. Of the four states, $|00\rangle$, $|01\rangle$, $|10\rangle$ and $|11\rangle$, which encode the two qubits, only the latter two are involved in this operation. Similar to the one-qubit case, these states are coupled to the intermediate state $|I\rangle$ which in turn is coupled to the additional shelving state $|S\rangle$.

Using the same state representation as before, we encode our states in the following ro-vibrational levels of Na_2: levels $|X, v = 0, J = 0\rangle$, $|X, v = 2, J = 0\rangle$, $|X, v = 2, J = 2\rangle$, $|X, v = 4, J = 2\rangle$ are used for the qubit basis states $|00\rangle$,$|01\rangle$,$|10\rangle$ and $|11\rangle$ respectively; then we use $|X, v = 4, J = 0\rangle$ for the shelving level and $|B, v = 3, J = 1\rangle$ as the intermediate

state. In this case each level except the ground state $|00\rangle$ couple strongly to the excited level. See Table 3.3 for the calculated energies and FC factors between the levels used in the simulation.

CNOT Gate

We present an explicit realization of a CNOT gate. The procedure developed here has obvious and immediate extension to other two-qubit gate operations (such as the SWAP or Controlled-Phase). Similarly, our method can be easily extended to 3-qubit gate operations, such as the Toffoli (Controlled-CNOT) gate. The pulse sequence of these composite gates thus generated is expected to be more efficient than the in tandem application of a sequence of the elementary gates.

After a CNOT gate operation, the initial two-qubit state of Eq. (3.17) transforms into

$$|\psi_f\rangle = \alpha_{00}|00\rangle + \alpha_{01}|01\rangle + \alpha_{11}|10\rangle + \alpha_{10}|11\rangle. \tag{3.18}$$

The implementation of this gate must therefore be able to achieve complete population transfer between the $|10\rangle$ and $|11\rangle$ states, without perturbing the coefficients of either the $|00\rangle$ or the $|01\rangle$ states. Because of the simple storage of qubits we have adopted, this task is reduced to simply exchanging the populations between two given ro-vibrational eigenstates within the same electronic manifold.

The use a one-photon π-pulse scheme is precluded because of the requirement in that scheme that the pulse area be *exactly* equal to π to obtain satisfactory (i.e., near 100 %) fidelity. Instead, we have devised a simple scheme capable of performing this operation using three APT processes (which are less sensitive to the pulse area) applied in tandem. The scheme, shown in Fig. 3.3, is similar to that used for the single qubit gates, with the three involved states coupling solely to the intermediate state $|I\rangle$. In the first stage one of the two upper qubit states, e.g., $|11\rangle$, undergoes an APT to the shelving eigenstate $|S\rangle$. As before, the pulses are applied in the "counter intuitive" order, first $\Omega_S(t)$ and then $\Omega_1(t)$, while

maintaining a significant overlap between them. Once the $|11\rangle$ state has been emptied, we transfer the population from $|10\rangle$ to $|11\rangle$, using pulses whose Rabi frequencies are Ω_1 and Ω_0. Lastly, to complete the procedure, the shelved population in $|S\rangle$ is transferred to the (now) vacant $|10\rangle$ state.

Our scheme requires the use of only three laser frequencies, with the overall gate fidelity being determined solely by the efficiency of each APT step. An implementation to the two-qubit SWAP gate or to the three-qubit CCNOT gate follows essentially the same scheme, save for the employment of different assignments for the qubit states, e.g., $|01\rangle$, $|10\rangle$ for the SWAP gate and $|110\rangle$, $|111\rangle$ for the CCNOT gate.

CNOT gate operation

Such a simulation is shown in Fig. 3.4. We begin with an initial state given by

$$|\psi_i\rangle = \frac{1}{\sqrt{7}}(|00\rangle + |01\rangle - 2|01\rangle + |11\rangle) \tag{3.19}$$

We use the scaled Rabi frequencies shown in Fig. 3.3.3, which are now entirely real, and introduce in each of the three APT process a relative Pump and Stokes phase difference of π in order to eliminate the extra π phase picked up by the target state due to the evolution [55]. The population of the states throughout the gate operation are shown in Fig. 3.4. We see that the population of state $|11\rangle$ is first transferred and stored in $|S\rangle$ and then the population of state $|10\rangle$ is transferred completely to state $|11\rangle$. Finally the population of state $|S\rangle$ is transferred to state $|10\rangle$. We note that the shelving state $|S\rangle$ is occupied for less than 100 ps, well below the spontaneous emission decay time. Notice that due to unwanted coupling effects the intermediate state periodically collects population for several ps, however this remains below the average cited decay time of such levels [9]. This effect also causes population leaking into the imaginary parts of the qubit coefficients, see Fig. 3.4.

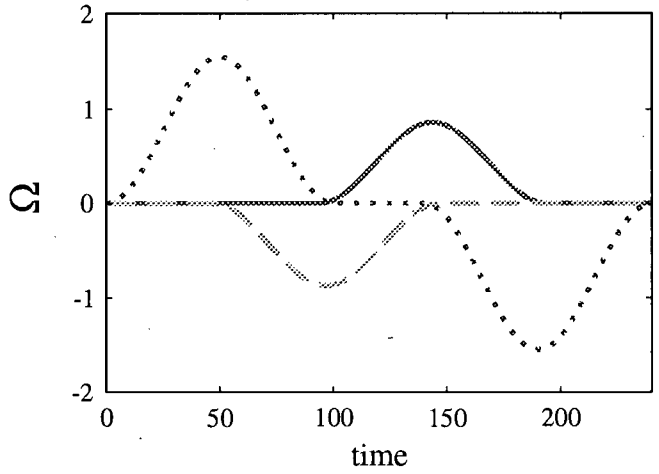

Figure 3.4: (a)

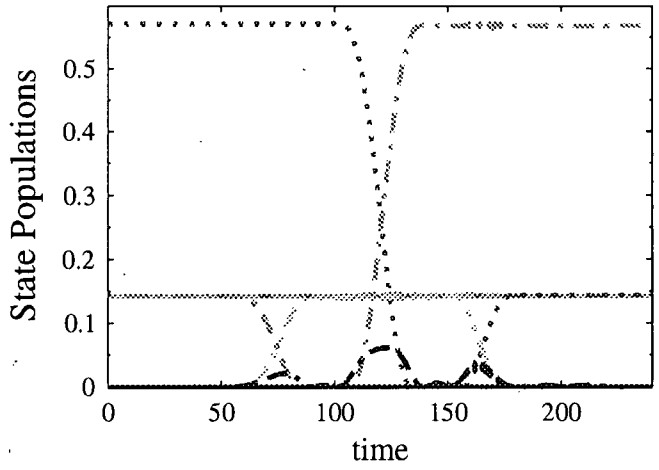

Figure 3.4: (b)

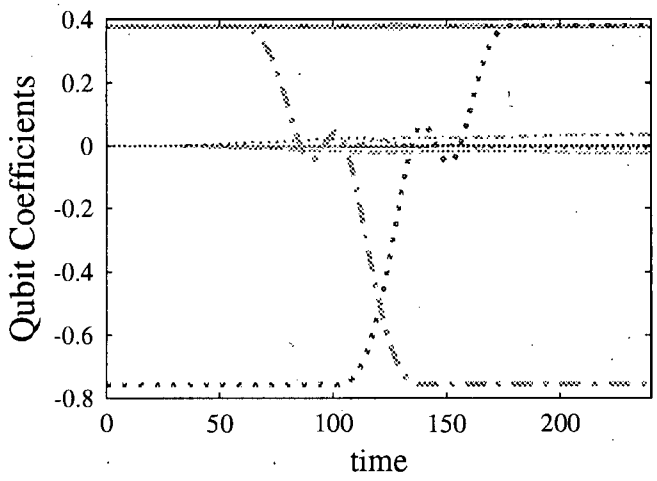

Figure 3.4: (c)

Figure 3.4: Numerical simulation of a CNOT gate implemented on a two-qubit system with an initial population split 1:1:2:1 between its four basis states. We use the same units as before. The same representation is used as in the previous plot. (a) Temporal profile of the Rabi frequencies of the pulses coupling each of the states to $|I\rangle$ for the three successive APT process required to implement this gate. Solid line: Ω_{10}. Dashed line: Ω_{11}. Dotted line: Ω_S. (b) Time evolution of the populations of the six states throughout the gate operation. These states are represented as $|00\rangle$ (solid line), $|01\rangle$ (dashed line), $|10\rangle$ (dotted line) and $|11\rangle$ (dot-dashed line), $|S\rangle$ (dash-dot-dot) $|I\rangle$ (dash-dash-dot) . The three independent APT processes between each of the states can be clearly seen. (c) The evolutions of the four qubit coefficients are shown using the same representation as in part (b). The thicker/thinner lines represent the real/imaginary parts of the coefficients.

As shown in the figure, the final state agrees exactly with the theoretical expectations. i.e., with

$$|\psi_i\rangle = \frac{1}{\sqrt{7}}\left(|00\rangle + |01\rangle + |01\rangle - 2|11\rangle\right) . \tag{3.20}$$

3.3.4 Composite Operations

In our encoding scheme, each of the possible combinations of qubits is assigned a single ro-vibrational level of a molecule. Therefore, in order to perform a particular one-qubit gate on each qubit of all N-qubit numbers, we must carry-out N of these one-qubit operations on

each of the appropriately selected 2^N levels. For instance, suppose we wish to apply a one-qubit phase gate, defined as before, on the *first* (right) qubit represented in our two-qubit system. This action will take our initial state from Eq. (3.17) to a final state

$$|\psi_f\rangle = \alpha_{00}|00\rangle + \alpha_{01}e^{i\phi}|01\rangle + \alpha_{10}|10\rangle + \alpha_{11}e^{i\phi}|11\rangle. \tag{3.21}$$

In this operation a phase ϕ has been added to each of the two two-qubit states whose *first* qubit is $|1\rangle$. If we had chosen the *second* qubit as the target then the $|10\rangle$ and the $|11\rangle$ states would have been multiplied by the $e^{i\phi}$ phase factor.

There are two basic options of implementing this and other one-qubit operations using our APT procedures in this two-qubit system :

1. One can perform two consecutive phase-gate operations for each of the two levels, using the same intermediate and shelving states for both processes.

2. One can introduce another intermediate and shelving state, $|I_2\rangle$ and $|S_2\rangle$, and then perform the two phase-gates simultaneously on both qubit states, as shown in Fig. 3.4.

The second option would appear preferable because it would consume half (or an N^{th}) the amount of time as the first option for a two (or N) qubit system. However, it is more restricted: Firstly, the laser pulses must be accurately constructed such that the appropriate levels are simultaneously coupled for each of the transitions, and secondly, the encoding of these states in the ro-vibrational eigenstates of the molecule must be chosen such that there is no interference between the two simultaneous processes. Thus, if we are to perform two simultaneous one-qubit operations in a two-qubit system, each of the two laser pulses will have to contain two different Rabi frequencies tuned to be in resonance with the transitions depicted in Fig. 3.4. In this scheme we first apply the two pulses $\{\Omega_{S1}, \Omega_{S2}\}$ followed by the $\{\Omega_{01}, \Omega_{11}\}$ pair, thereby simultaneously transferring the populations of the the $|10\rangle$ and $|11\rangle$ states to the two shelving levels, $|S_1\rangle$ and $|S_2\rangle$ respectively. Then, as before, this pulse sequence is reversed and the populations are sent back with the desired phase to their original levels.

In the N-qubits systems, N different narrow-band pulses must be contained within each pulse envelope in order to simultaneously perform the N single qubit operations. Experimentally, we can design such pulses using commercially available pulse shapers. The above strategy also applies to the Hadamard and other one-qubit gates.

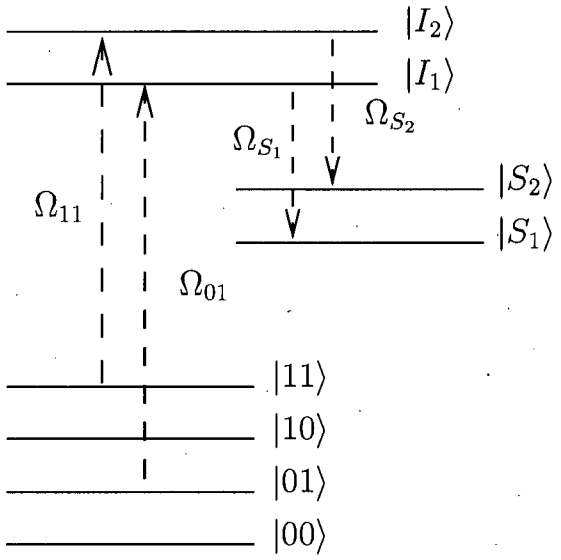

Figure 3.4: Illustration of the pulses used for a one-qubit phase gate applied to the first (right) qubit in a two-qubit system. Since two one-qubit operations are being performed simultaneously, there are two intermediate, $|I_1\rangle$,$|I_2\rangle$, and two shelving states, $|S_1\rangle$,$|S_2\rangle$, in addition to the two-qubit basis states. Each of the two pulse envelopes contains two frequencies, $\{\Omega_{01}, \Omega_{11}\}$ and $\{\Omega_{S1}, \Omega_{S2}\}$, which address the appropriate levels for the two APT processes.

We now apply our technique to perform composite operations made up of the phase-change, Hadamard, and CNOT logic gates on two-qubit systems, thereby proving its ability to perform any desired quantum computation on qubit systems of arbitrary dimensions. Instead of demonstrating again the $\pi/8$-phase gate we study the π-phase change gate, which involves simply adding a different phase to one of the pulses in the second APT process, as discussed in Section 2.2.2. We show that one can produce in this way a molecular representation of a Bell state with essentially 100% fidelity. Here we use the same molecular state encoding as in the CNOT example with values shown in Table 3.3, with the additional

shelving ($|S_2\rangle$) and intermediate state ($|I_2\rangle$) encoded in the $|X, v = 0, J = 2\rangle$ and $|B, v = 1, J = 1\rangle$ states respectively.

State	Quantum #	Energy (a.u.)	FC factor ($\|I_1\rangle$)	FC factor ($\|I_2\rangle$)
$\|00\rangle$	$\|X, 0, 0\rangle$	-0.0267275	0.2638	0.
$\|01\rangle$	$\|X, 0, 2\rangle$	-0.0267229	0.2640	0.
$\|S_1\rangle$	$\|X, 2, 0\rangle$	-0.0253013	0.5219	-0.19081
$\|S_2\rangle$	$\|X, 2, 2\rangle$	-0.0252891	0.5221	-0.1912
$\|10\rangle$	$\|X, 4, 0\rangle$	-0.0239035	0.	-0.1974
$\|11\rangle$	$\|X, 4, 2\rangle$	-0.0238893	0.	-0.1970
$\|I_1\rangle$	$\|B, 1, 1\rangle$	0.0654244	X	X
$\|I_2\rangle$	$\|B, 3, 1\rangle$	0.0665435	X	X

Table 3.3: Energies and FC factors of the levels in Na_2 used for the gate simulations on the 2-qubit system.

Multiple-Gate Operations

In Fig. 3.5 we present simulations of three consecutive gate operations on a *product* initial state:

$$|\psi_i\rangle = \frac{1}{2}\left(|0_1\rangle + |1_1\rangle\right)\left(|0_2\rangle + |1_2\rangle\right) = \left(|00\rangle + |01\rangle + |10\rangle + |11\rangle\right). \tag{3.22}$$

The first operation performs a π-phase gate on the *first* (left) qubit if this qubit is 1, resulting in the state

$$|\psi_m\rangle = \frac{1}{2}\left(|00\rangle + |01\rangle - |10\rangle - |11\rangle\right). \tag{3.23}$$

The two individual phase-gate operations that must be performed on the $|01\rangle$ and $|11\rangle$ states are separated for demonstration. However, since these procedures can be done simultaneously by tuning the pulses to address each of the appropriate levels we used different intermediate, $|I_1\rangle$, $|I_2\rangle$, and shelving states, $|S_1\rangle$, $|S_2\rangle$, for each case.

$$|\psi_f\rangle = \frac{1}{\sqrt{2}}\left(|00\rangle - |11\rangle\right). \tag{3.24}$$

In the next step a Hadamard gate acts on the second (right) qubit of $|\psi_m\rangle$. Shown in

Fig. 3.3.4 are the two consecutive single qubit processes: $|00\rangle + |01\rangle \rightarrow |00\rangle$ and $-(|10\rangle + |11\rangle) \rightarrow -|10\rangle$ that together give us the state

$$|\psi_n\rangle = \frac{1}{\sqrt{2}}(|00\rangle - |10\rangle). \tag{3.25}$$

Finally, we apply a CNOT gate, moving the population from $|10\rangle$ to $|11\rangle$. Since the target state did not contain any population, the shelving state was not required. (In fact a basic three-level APT transfer scheme would have been sufficient.) The final operation leaves us in a representation of a Bell state

This combined logic operation is characterized by the same essentially-perfect gate fidelity encountered for each of the individual gates. A calculation finds an error of less than 0.01% for this process, the slight deviation from previously higher-stated fidelities are due to the large variations in Rabi frequencies between pulses that we use in order to test the robustness of the scheme. Higher accuracy, approaching the presumed fault-tolerant error threshold of 99.99 %, can be obtained by minor tuning of the pulse intensities together with an additional lengthening of the pulses conjoining each of the consecutive APT processes.

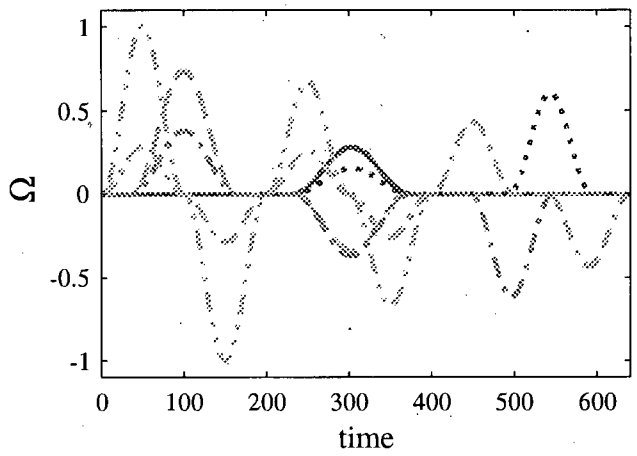

Figure 3.5: (a)

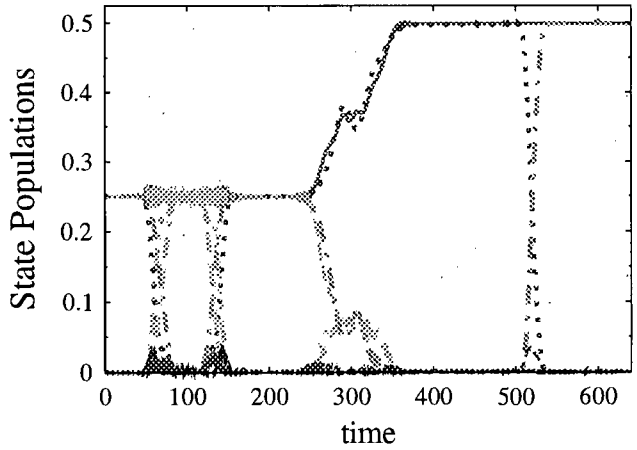

Figure 3.5: (b)

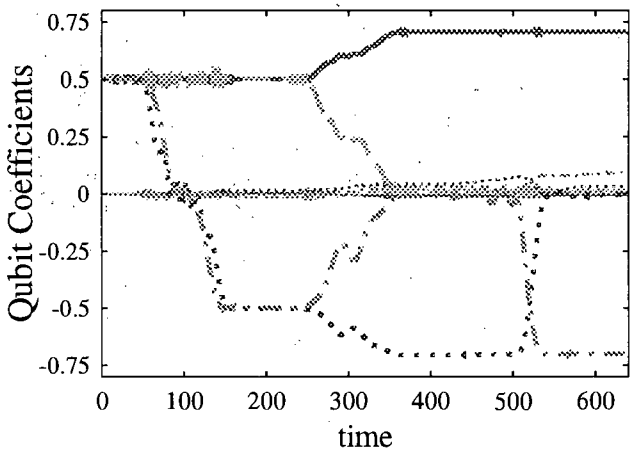

Figure 3.5: (c)

Figure 3.5: Results from the numerical simulation of the three discussed gates, constituting a universal gate set, applied to our two-qubit system initialized to an even superposition of the four qubit basis states. Two consecutive pulse sequences are applied to the appropriate levels to perform each of the two single-qubit gate operations. The units used are as before. (a) Plot of the Rabi frequencies for the pulses coupling each one of the states: $|00\rangle$ (solid), $|01\rangle$ (dashed), and $|S_1\rangle$ (dash-dot-dot) to the intermediate state $|I_1\rangle$; and $|10\rangle$ (dotted), $|11\rangle$ (dash-dot), and $|S_2\rangle$ (dash-dash-dot) $|I_2\rangle$. (b) Time evolution for each states population. We use a similar representation as in Fig.3.4 with changes to the state $|S_2\rangle$ (dash-dash-dot), and the two intermediate levels (thin solid lines) whose population fluctuate near zero. (c) The evolutions of the four qubit coefficients are shown using the same representation as before. The thicker/thinner lines represent the real/imaginary parts of the coefficients.

3.3.5 Remarks

We have developed a method of implementing a universal gate-set on a one- and two-qubit molecular systems using APT. We have demonstrated the procedure using the Na_2-molecule vibrational states. Our method is robust and produces nearly flawless gate fidelities. The procedure can be readily extended to perform any quantum computation on much larger systems. An experimental realization of our procedure in the Na_2 molecule is now being developed.

We have shown that when the number of qubits is increased it is possible to shorten the

performance times by using more molecular levels. Although this shortening of performance times uses more resources (molecular levels), it enables *multiplexing* and saving in *laser* resources, because the procedure then uses fewer pulses, with each pulse being composed of many narrow band components. Such pulses can now be readily prepared using commercially available pulse shapers.

Although we have shown how to produce a molecular representation of a Bell state, we have so far not *exploited* the theoretically-predicted superior scaling of entangled states. In molecular systems, entanglement of the vibrational and rotational quantum states in an ordinary optical excitation process is easily attainable via broadband excitations from a $|v_i\rangle|J_i\rangle$ initial state to produce an entangled superposition of energetically close $|v'\rangle|J_i+1\rangle$ and $|v'\rangle|J_i-1\rangle$ states. The exploitation of such entanglements in conjunction with our procedures is now being investigated.

Due to the restrictions imposed by the adiabatic conditions on the implementation of the gate operations, the durations of the pulses are limited to, at minimum, the picosecond time scale. The necessary intensities of the fields for faster pulse which fulfill the traditional conditions for adiabaticity would be disastrous in a molecular system such as the sodium dimer, does that imply that the use of femtosecond pulses in molecular system will forever be held within a coherent control strategy? Or is it possible to use such broadband pulses in an adiabatic manner, and thus provide a speed-up of the quantum gate operations while retaining the robustness inherent in adiabatic processes? If so then larger algorithms become feasible since more operations can be performed before the relaxation of the states affect the coherence of the qubits

Chapter 4

Piecewise Adiabtic Passage with a Series of Femtosecond Pulses

4.1 Coherent Control versus Adiabatic Passage

In the past couple of decades two strategies have emerged as being the most useful for achieving quantum control. These are: coherent control (CC) with broad and narrow band laser pulses [55] and "Adiabatic Passage"[20, 39]. Control with broadband pulses relies on the possibility to shape the pulses both in the time and frequency domains [1]. This enables the realization of various CC schemes [55] that utilize coherent laser radiation to induce interferences between indistinguishable quantum pathways. One can enforce the desired evolution of a quantum system with high accuracy due to the ability to control quantum interferences. Though applicable to a wide range of problems, control with ultrashort pulses is often highly sensitive to the durations and exact shapes and intensities of the laser fields used.

Adiabatic passage (AP) is a complementary control strategy that enables the execution of complete population transfer between quantum states, using pulses that are long on the time scale of the system's evolution. As demonstrated in the previous chapters the AP approach, when exercised in the context of bound-bound [20, 39, 43], and even bound-free [71] transitions, can bring about very high yields, often approaching unity. In contrast to control with shaped pulses, the AP method is highly robust with respect to variations in the durations and amplitudes of the laser pulses used [12, 20, 39]. Unfortunately, the long pulse lengths pose a restriction on the rate of a contral process, which can limit its uses in certain

applications such as quantum computation. For large scale quantum operations, fast gate operations are essential to avoid decoherence due to decay or other interacting phenonema. Moreover, the adiabaticity condition requires slowly changing field envelopes which are hard to shape due to their narrow spectral bandwidth. This limits the set of quantum control tools and the range of achievable goals of AP.

Here we propose a way of merging the strategies of adiabatic passage and the control with shaped pulses (for a review of complementary ways of combining AP with CC see Ref. [34]). We do so by performing the population transfer in a piecewise manner using a series of femtosecond pulses. Our technique is endowed with both the robustness of AP and the flexibility afforded by the use of broadband light sources. The following work extends the concepts of "Coherent Accumulation" [63] and the Ramsey experiment [47], where a slow process is implemented in a piecewise manner using a train of short, mutually coherent, laser pulses.

4.2 STIRAP on the Sodium atom

As our primary example we consider below the Stimulated Raman Adiabatic Passage (STIRAP) [20, 39] scheme, see Section 2.1.3. For a brief review, we say in its simplest version, that population from an initial quantum state $|1\rangle$ is transferred to a target state $|3\rangle$ via an intermediate state $|2\rangle$ by means of two narrow-band laser pulses: the "pump" $E_p(t) \equiv Re\{\varepsilon_p(t)e^{-i\omega_p t}\}$, tuned on resonance with the $\epsilon_2 - \epsilon_1$ transition and the "dump" $E_d(t) \equiv Re\{\varepsilon_d(t)e^{-i\omega_d t}\}$, tuned on resonance with the $\epsilon_3 - \epsilon_2$ transition. We describe the system under the rotating wave approximation in the interaction representation [20, 39, 55]; thus when both laser fields are turned off, the state amplitudes do not evolve. In the presence of the laser fields, the "null vector" is

$$|\Psi_0\rangle = \sin\theta|1\rangle - \cos\theta|3\rangle, \qquad \tan\theta = \Omega_d/\Omega_p^* , \tag{4.1}$$

where $\Omega_p(t) \equiv \mu_{2,1}\varepsilon_p(t)$ and $\Omega_d(t) \equiv \mu_{2,2}\varepsilon_d(t)$, μ_{ij} being the dipole matrix elements. If, at the beginning of the process, we set $|\Omega_d| > 0$ and $\Omega_p = 0$ and at the end we let $|\Omega_p| > 0$ and $\Omega_d = 0$ (the "counter-intuitive" pulse ordering [20, 39]), the null vector will evolve from state $|1\rangle$ to state $|3\rangle$ without ever populating the intermediate state $|2\rangle$. The wave function $|\Psi(t)\rangle$ will follow the null vector, making an adiabatic passage from $|1\rangle$ to $|3\rangle$. The particular values of the Rabi frequencies do not matter as long as we meet the adiabaticity condition [20, 39]

$$|\dot{\theta}| \ll \sqrt{|\Omega_p|^2 + |\Omega_d|^2} \,. \tag{4.2}$$

Fig. 4.1(a,b) shows a computation for an ordinary ("reference") AP for $|1\rangle$ = 3s, $|2\rangle$ = 3p, and $|3\rangle$ = 3d electronic states of the Na atom, using the empirically derived $\mu_{i,j}$ matrix elements [1]. The energy levels of the states were taken from the same source, the energies of the $3p$ and $3d$ states relative to the zeroed ground state $3s$ are 0.07731 and 0.13292 Hartrees respectively. In Fig. 4.1(a,b) we use two circularly polarized laser pulses with sine-squared $\varepsilon_{p(d)}$ field envelopes and temporal duration of 0.75 ps (FWHM in amplitude). The pulses are applied with a 0.6 ps delay and have central wavelengths $\lambda_p = 2\pi c/\omega_p$ = 589 nm and $\lambda_d = 2\pi c/\omega_d$ = 819 nm. Each pulse is capable of driving about three Rabi oscillations within the time pump-dump overlap, satisfying the conditions for adiabaticity. We observe a complete transfer of population from the state $|1\rangle$ to the state $|3\rangle$, while never significantly populating the state $|2\rangle$. Note that in the counter-intuitive ordering, only the overlapping region of the pulses is important, since the population of the states does not change when only one of the pulses is present.

4.3 Piecewise Adiabatic Passage

We now modify the above scenario by letting the material system evolve according to the above scheme until time t_1, at which point both laser fields are abruptly turned off. At some

[1] NIST Atomic Spectra Database, http://physics.nist.gov/PhysRefData /ASD/ . We took μ_{12} = 2.5 a.u., and μ_{23} = 3 a.u. The field-free decay is not relevant at the time scales discussed. Ionization by the field was not taken into acount in the calculations shown in the paper; it was estimated to be negligible in the single-photon PAP, and to reach the level of ~10-15% in the (2+1) process.

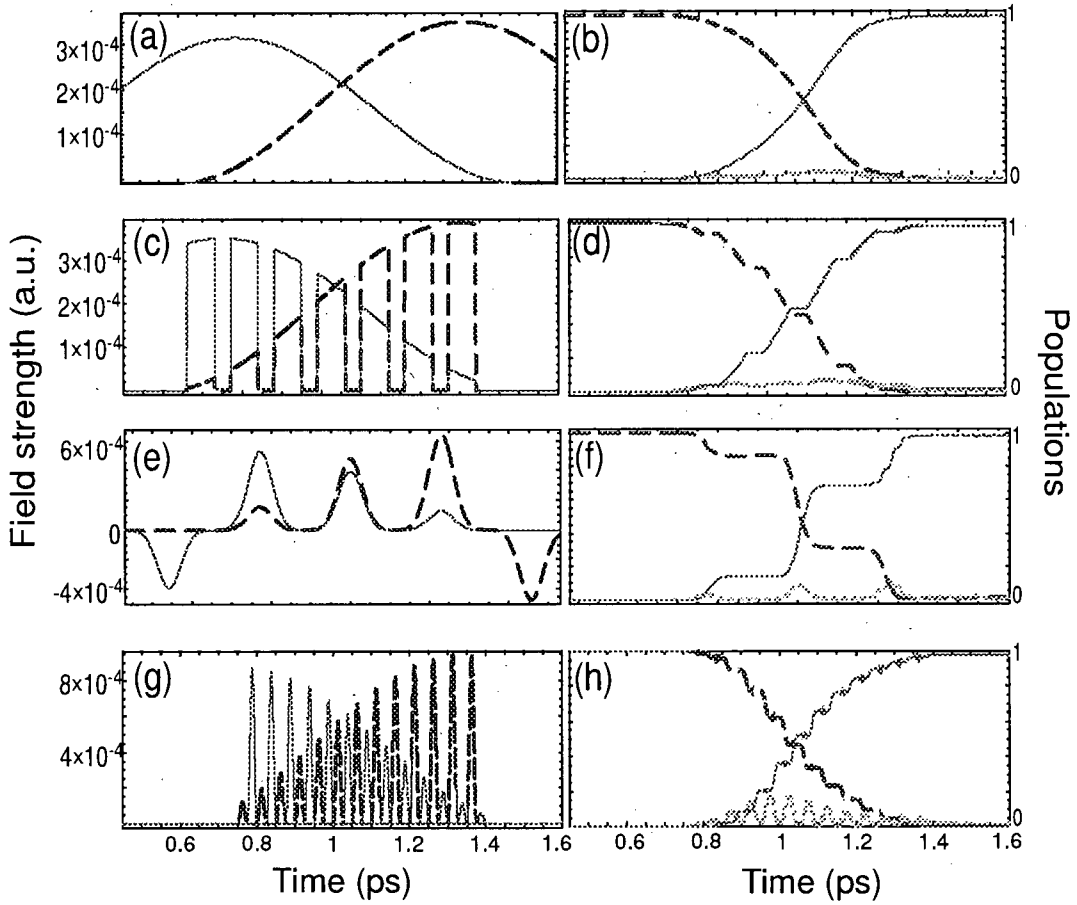

Figure 4.1: Four types of PAP processes: (a,c,e,g) - the pulse sequences; dashed blue - the pump, firm red - the dump. (b,d,f,h) - the populations ($|b_i(t)|^2$); dashed blue - $i = 1$, dotted green - $i = 2$, firm red - $i = 3$. (a,b): The reference AP; (c,d): PAP with sharp turn-ons and turn-offs; (e,f) and (g,h): PAP with smooth overlapping and non-overlapping pulses.

later time t_2, we abruptly turn both fields back on, making sure that the absolute phase of each field is retained, i.e. the relative phase of the carrier oscillations after t_2 and before t_1 is zero; this we will call the *absolute phase condition*. Since the coefficients $b_i(t)$ do not evolve during the zero-field period, $b_i(t > t_2)$ continue to follow the adiabatic passage with $b_i(t_1) = b_i(t_2)$ serving as a new starting point. Repeating the turn-off/turn-on many times allows us to execute the AP process in a controlled piecewise manner.

Fig. 4.1(c,d) demonstrates the action of a pulse sequence obtained by turning off the original reference STIRAP fields at periodic intervals, while scaling up $\varepsilon_{p(d)}(t)$ during the "on" periods, as described in detail below. As shown, the resulting pulse sequence closely reproduces the effect of an ordinary AP. Moreover, we find that this "Piecewise Adiabatic Passage" (PAP) procedure is insensitive to the particular shape and strength of the pulses, as well as to the durations of the "off" periods. The absolute phase condition ensures the insensitivity of the scheme to the "off" periods if both fields are on exact resonance; this is not true for non-zero field detunings.

A more practical application demonstrating a soft turn-on/turn-off version of PAP is shown in Fig. 4.1(e,f) and (g,h). In panels (e,f) the pump and the dump laser fields are obtained by the spectral phase shaping of 75 fs pulses:

$$\varepsilon_{p(d)}^{shaped}(\omega) = \varepsilon_{p(d)}^{unshaped}(\omega)\, F_{p(d)}(\omega), \tag{4.3}$$

where $F_{p(d)}(\omega) = \exp\left\{i\, A_{p(d)} \sin[\Delta T(\omega - \omega_{p(d)})]\right\}$ with $A_{p(d)} = \mp 1.2$, and $\Delta T = 229$ fs. The resulting pulse sequence, shown in Fig. 4.1(e), is comprised of copies of the original transform-limited femtosecond pulse of duration τ separated in time by ΔT, and with smoothly changing amplitudes defined by the value of A [75]. We see that the soft turn-on/turn-off PAP is as successful in bringing about the desired population transfer as the abrupt turn-on/turn-off version discussed above. The negative field envelopes (opposite sign of the field) in Fig. 4.1(e) do not influence the population transfer, and are due to the sinusoidal phase modulation of the spectrum [75].

4.4 Preliminary Theory

It is instructive to consider each pump-dump segment of the combined pulse train as a deviation from the smoothly varying reference AP field as shown in Fig. 4.1(a). We do so by writing the interaction Hamiltonian as

$$H(t) = H_0(t) + H_1(t), \quad \text{where} \quad H_0(t) \equiv -\mu \cdot E_0(t), \qquad (4.4)$$
$$\text{and} \quad E_{0\,p(d)}(t) = Re\{\varepsilon_{0\,p(d)}(t)\exp(-i\omega_{0\,p(d)}t)\}$$

is the field from the reference Hamiltonian. The evolution operator in PAP will be equal to that in the reference AP, if

$$\begin{aligned} S_n &= \mathcal{T}\exp\left[-i\int_{t_n-\tau/2}^{t_n+\tau/2} H_0(t)dt - i\int_{t_n-\tau/2}^{t_n+\tau/2} H_1(t)dt\right] \\ &= \mathcal{T}\exp\left[-i\int_{t_n-\tau/2}^{t_n+\tau/2} H_0(t)dt\right] \equiv S_{0n}, \end{aligned} \qquad (4.5)$$

where $\mathcal{T}$ denotes the time ordering operator and S_{0n} is the evolution operator of the reference AP during the n^{th} segment of duration τ. By requiring $\int_\tau H dt = \int_\tau H_0 dt$, condition (4.5) can be satisfied within the first order of the shake-off perturbation theory [13] with respect to $\varpi\tau$, where $\varpi \sim \Omega_{p,d}$ is the typical transition frequency in the dressed Hamiltonian. Therefore, in each segment we can replace the reference Hamiltonian H_0 by a piecewise H of the same area, as long as each of the fields drives no more than a fraction of a Rabi cycle in that segment.

Within the same level of accuracy, the actions S_n and S_{0n} are composed of independent actions of the pump and dump fields. In order to enforce condition (4.5), we require that $\int_\tau \varepsilon_{p(d)}dt = \int_\tau \varepsilon_{0\,p(d)}dt \simeq \varepsilon_{0\,p(d)}(t_n)\tau$. Constructed this way, the field of the pulse train is only defined by the coarse-grained $\varepsilon_{0\,p(d)}(t_n)$ profile, and is insensitive to its short-time behavior. At the same time, since the pulse area of the reference AP satisfies the adiabaticity condition, so does the area of the PAP pulse train. Thus constructed PAP is as robust to

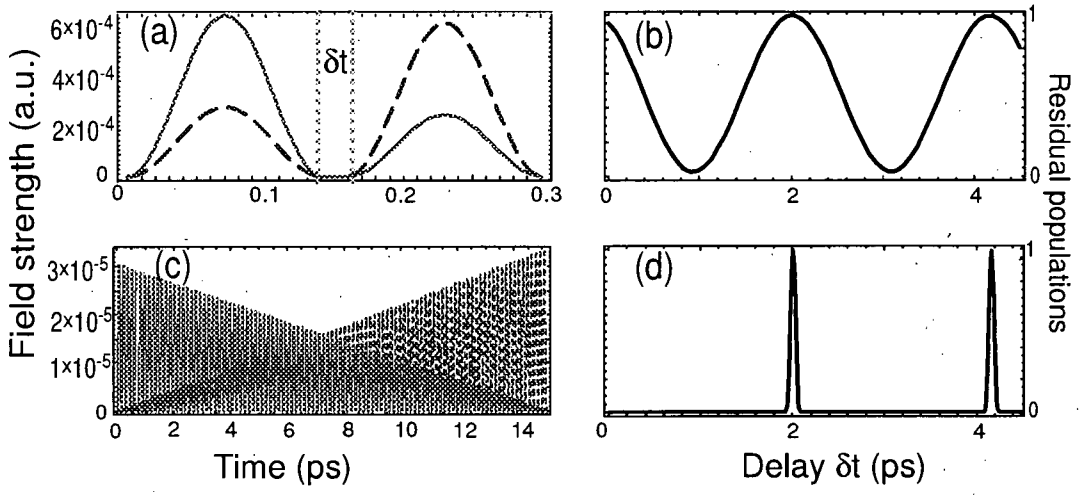

Figure 4.2: Ramsey interference in PAP. (a,c): The field envelopes of the pump (dashed blue) and dump (red) pulse sequences. The green dotted lines in panel (a) mark the onset of the turn-off period(s). (b,d): The final $|b_3|^2$ population as a function of the duration of the turn-off period(s).

the particular choice of $\varepsilon_{0\,p(d)}(t_n)$ as the reference AP.

Effective coarse-graining of the evolution (Eq. (4.5)) explains the observed robustness of the transfer both to the pulse shapes, and to additional noise in the pulse envelopes (for an analysis of noise effects in a conventional STIRAP, see Ref. [49]). The discretized coarse-grained description is complementary to the search of the generalized Floquet states of Ref. [77], and can help in deriving conditions of complete population transfer without relying on the particular field spectrum.

4.5 Ramsey Interference

The phases of the pump and dump pulses can be used in PAP as additional control knobs. Similar to the Ramsey interference effect [47], if either one or both fields are detuned off the exact resonance, the probability transfer in PAP becomes sensitive to the duration of the turn-off periods. In Fig. 4.2(a) we show PAP performed with just two pairs of (75 fs) pump and dump pulses inducing one-photon transitions between the levels 3s, 3p, and 3d of Na.

Panel (b) depicts the final population of the state 3d as a function of the duration of the turn-off periods δt. Fig. 4.2(c,d) shows the same results for the pulse trains composed of 100 segments with linearly increasing (decreasing) pump (dump) field strengths. The dump wavelength was set to ~818 nm, 1 nm away from the exact 3p-3d resonance.

We first note that even as few as two pairs of pulses suffice to reproduce the effect of conventional AP. It can also be seen in Fig. 4.2(b) and (d), that there is a strong dependence of the final state population on the duration of the turn-off period(s). The sharp peaks seen in the latter case are analogous to the Ramsey fringes: the longer the pulse trains the narrower the fringes. This suggests that applying PAP, implemented with a frequency-comb source [78], to a metastable target state might present a useful alternative to the precision measurements of atomic transitions and frequency standards.

There is an underlying connection between PAP and the coherent accumulation schemes studied in Ref. [63]. Consider the example shown in Fig. 4.1(g,h) in which the pump and dump pulses do not overlap. Within each non-overlapping pulse pair, the pump first drives the population into the intermediate level, from which it gets subsequently dumped into the target state. We have ascertained numerically that the accumulating action of this coherent non-overlapping scheme is insensitive to the intensity of the pump and dump trains, as long as their envelope mimics that of the reference AP. Unlike the preceding examples, the population is transferred, in small portions, via the intermediate level. Yet, similarly to PAP with overlapping pulses, the transfer is complete and robust due to the effective coarse graining.

4.5.1 Classical Analogue

Here is a technique that can be used in generalizing the quantum adiabatic passage. It is neither adiabatic in the traditional sense, nor, strictly speaking, quantum. Here we begin with a simple classical model.

I. Evolution of a point on a sphere.

Consider the evolution of a point on a unit sphere under a train of alternating rotations. The rotations are: first, by the small angle α_P about the z axis; then, by the small angle α_D about the x axis. That is,

$$\begin{pmatrix} x_{n+1} \\ y_{n+1} \\ z_{n+1} \end{pmatrix} = \hat{\mathrm{D}}_n \hat{\mathrm{P}}_n \begin{pmatrix} x_n \\ y_n \\ z_n \end{pmatrix} \tag{4.6}$$

where:

$$\hat{\mathrm{P}}_n \equiv \mathrm{R}_z(\alpha_P) = \begin{pmatrix} \cos\alpha_P & -\sin\alpha_P & 0 \\ \sin\alpha_P & \cos\alpha_P & 0 \\ 0 & 0 & 1 \end{pmatrix},$$

$$D_n \equiv \mathrm{R}_x(\alpha_D) = \begin{pmatrix} 1 & 0 & 0 \\ 0 & \cos\alpha_D & -\sin\alpha_D \\ 0 & \sin\alpha_D & \cos\alpha_D \end{pmatrix}. \tag{4.7}$$

The values of the angles α_P and α_D may also depend on the number n, however this will not be analyzed here. The product of the two operators, $\hat{\mathrm{D}}_n$ and $\hat{\mathrm{P}}_n$, gives us a unitary matrix

$$U_n = \hat{\mathrm{D}}_n \hat{\mathrm{P}}_n = \begin{pmatrix} \cos\alpha_P & -\sin\alpha_P & 0 \\ \sin\alpha_P\cos\alpha_D & \cos\alpha_P\cos\alpha_D & -\sin\alpha_D \\ \sin\alpha_P\sin\alpha_D & \cos\alpha_P\sin\alpha_D & \cos\alpha_D \end{pmatrix}, \tag{4.8}$$

which, by Euler's rotation theorem, is simply a rotation by an angle, known as Euler's angle, about some axis, called the Euler axis [21]. All rotation matrices U_n (i.e. elements of SO_3) have eigenvalues given by $\{1, exp(\pm i\alpha_0)\}$, where α_0 defines the Euler angle. Futhermore, the eigenvector corresponding with the eigenvalue of 1 is invariant under rotation and, if non-zero, thus defines the Euler axis (up to a factor of ± 1). Therefore, as defined, U_n rotates

a vector $(x, y, z)^T$ by an angle α_0 found to be equal to

$$\cos\alpha_0 = (\cos\alpha_P + \cos\alpha_D + \cos\alpha_P \cos\alpha_D - 1)/2. \tag{4.9}$$

The Euler axis about which the rotation occurs can be represented by two angles: a polar ($0 \leq \theta_0 \leq \pi$) and an azimuthal ($0 \leq \phi_0 \leq 2pi$) angle, where

$$\phi_0 = -\alpha_P/2, \qquad \tan\theta_0 = \sqrt{\tan^2(\alpha_D/2)/\sin^2(\alpha_P/2)}\ . \tag{4.10}$$

Assuming α_P, α_D, α_0 are small angles, we can approximate the above equations by an expansion to first-order in those variables, obtaining

$$\alpha_0 \approx \sqrt{(\alpha_P{}^2 + \alpha_D{}^2)}, \tag{4.11}$$

$$\phi_0 \approx -\alpha_P/2, \tag{4.12}$$

$$\tan\theta_0 \approx \alpha_D/\alpha_P\ . \tag{4.13}$$

To verify, notice that if $|\alpha_D| > 0$ and $\alpha_P = 0$ the axis of rotation of the sphere coincides with the x axis, as expected. Secondly, if $|\alpha_P| > 0$, $\alpha_D = 0$, then the axis of rotation coincides with the z axis. We shall characterize the dynamics of a point on the sphere by its polar coordinates ($\theta(n)$, $\phi(n)$), where n represents the n^{th} small rotation.

First, let's consider the situation when the values of α_P, α_D are constant throughout the sequence of rotations. Under the sequence of U_n, every point on the sphere will perform rotations around the point (θ_0, ϕ_0), thus the point with the initial coordinates (θ_0, ϕ_0) remains fixed. This is the stable point of the dynamical map generated by the sequence of U_n. Any point whose initial coordinates are ($\theta(0)$, $\phi(0)$) or are in the neighbourhood of (θ_0, ϕ_0) will remain in that vicinity.

Now consider the situation when the values of α_P, α_D vary very slowly throughout the sequence of U_n. Then the stable point (θ_0, ϕ_0) slowly moves on the sphere. Specifically, if initially $\alpha_P = 0$, and at the end $\alpha_D = 0$, then the stable point slowly moves, near the

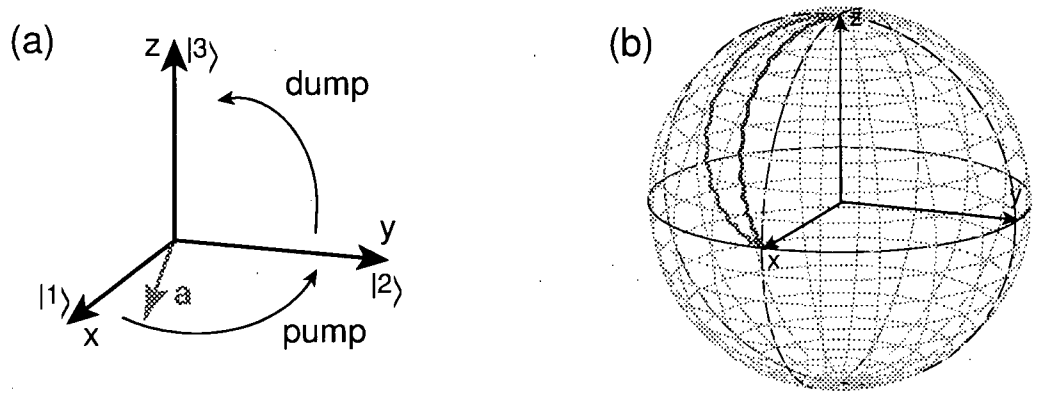

Figure 4.3: Classical representation of PAP. (a): Depiction of the state vector **a**. (b): Two sample trajectories of the **a** vector during the PAP process. Both the pump and the dump sequences of small rotations rotate the vector by an overall angle of $10\times 2\pi$. The left (right) trajectory corresponds to 50 (100) pulses in each sequence.

zeroth meridian, from the intersection of the x axis with the sphere, to the z axis. Observe the evolution of a point, initially given by the coordinates $(\theta(0), \phi(0))$ that are close to the x axis. If (i) the angles α_P, α_D remain small and non-commensurable to 2π, and (ii) the motion of the stable point (θ_0, ϕ_0) is slow compared to rotations of $\theta(n)$, $\phi(n)$ around (θ_0, ϕ_0), then, by classical adiabaticity, the point $(\theta(n), \phi(n))$ will follow (θ_0, ϕ_0). At the end of the sequence it will lie close to the z axis. Its trajectory on the sphere is expected to remind a cycloid lying slightly off the zeroth meridian - a trace of small-radius rotations around the moving center. Fig. 4.3(a) shows two typical examples of such trajectories, confirming our assumption.

The condition (ii) of the "coarse-grained adiabaticity" in the above paragraph implies: the change of the angle θ_0 during one period of rotation of $(\theta(n), \phi(n))$ around (θ_0, ϕ_0), equal to $2\pi/\alpha_0$, is much less than 2π. That is,

$$\Delta\theta_0 \ll \sqrt{(\alpha_P{}^2 + \alpha_D{}^2)/2}, \tag{4.14}$$

II. Relation to PAP

An analogy can be make from the classical picture discussed above to our PAP scheme by considering a very informative, though, in general, incomplete, description of the quantum system. This is given by following the trajectory of the amplitudes of vector **a** shown in Fig. 4.3(a) [20, 28, 39]. Assuming Ω_p and Ω_d are real, and if at time $t = 0$ we have $b_1 = 1$ and $b_2 = b_3 = 0$, then we may represent the vector $\mathbf{a} = (\mathbf{a}_x, \mathbf{a}_y, \mathbf{a}_z)$ as follows: $\mathbf{a}_x = \mathrm{Re}(b_1)$, $\mathbf{a}_y = -\mathrm{Im}(b_2)$, and $\mathbf{a}_z = \mathrm{Re}(b_3)$, since the phase of all the states will remain constant. Now each pump pulse, transferring populations between states $|1\rangle$ and $|2\rangle$, will rotate **a** by a small angle $\alpha_P = \int_\tau \Omega_P^*(t)dt$ about the z-axis. Likewise, each dump pulse will rotate **a** about the x axis by an angle $\alpha_D = \int_\tau \Omega_D(t)dt$. This combination of these two rotations result in an overall rotation of **a** by an angle α_0 about an axis defined by the (θ_0, ϕ_0) polar and azimuthal angles, given in their lowest-order expansion in the angles α_P and α_D as shown in Eq. (4.11). As $\Omega_{p(d)}(t)$ evolve, the otherwise stable (θ_0, ϕ_0) vector, which coincides with the null vector of our reference AP in the limit of small pulse areas (see Eq.(4.1)), moves slowly from being aligned along the x axis to being aligned along the z axis. As shown in Fig. 4.3, as long as the individual α_P and α_D are small, the **a** vector will faithfully follow the (θ_0, ϕ_0) null vector. This trajectory of the vector **a** on the sphere of states, composed of piecewise rotations around the moving center (θ_0, ϕ_0), resembles a cycloid. Coarse-grained adiabaticity can be shown to be guaranteed as long as the adiabaticity condition, see Eq.(4.14), holds. In the limit of small rotations, this condition reduces, up to an insignificant numerical factor, to the adiabaticity condition from Eq. (4.2) of conventional AP.

We thus expect the overall evolution to be robust as long as Eq.(4.14) is satisfied and the α_P, α_D angles at each step are small. These expectations were verified numerically for various sequences of alternating rotations with slowly varying amplitudes. Fig. 4.3(b) depicts two such trajectories. Each of them starts at the state $|1\rangle$ and follows the AP route slightly outside the zeroth meridian (i.e., somewhat populating state $|2\rangle$) to coincide finally with state $|3\rangle$.

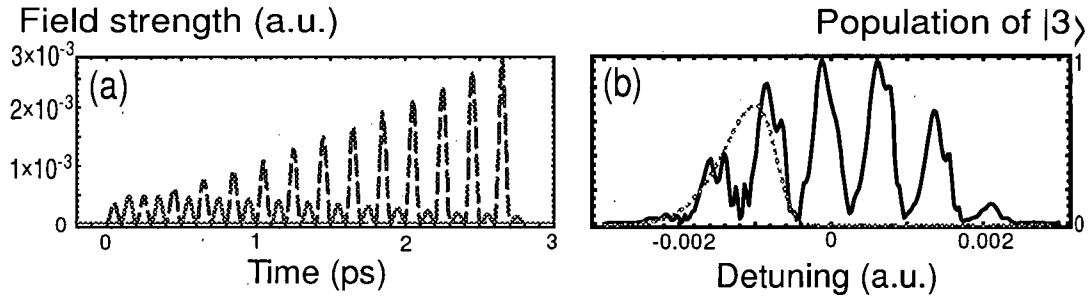

Figure 4.4: Field envelopes of the (2+1) PAP, and the final population of the target state as a function of the dump detuning in PAP (black), and in the reference conventional STIHRAP (dashed red).

4.6 2+1 Photon STIRAP

The ability to alternate between the pump and dump segments can be useful in minimizing deleterious effects of the Stark shifting of levels. This is particularly the case in the two-photon + one-photon ("2+1") Stimulated Hyper-Raman Adiabatic Passage (STIHRAP [15, 16, 27, 66]), whose implementation with short laser pulses is considered very difficult due to the strong time-dependent AC Stark shifts of the levels. Although one can transfer the population into the target level by detuning both the pump and the dump lasers from the exact resonance [15, 16, 27, 66], the robustness of the method is strongly reduced since the conditions connecting the field-induced Stark shifts with the required frequency offsets are stringent.

We have considered the action of strong pump pulses which drive a two-photon transition from the ground state of Na (3s) to an intermediate state 4s, while the dump pulses cause a one-photon down-transition from 4s to the target state 3p. Fig. 4.4(a) shows the pulse sequence with non-overlapping pump and dump segments which drives the (2+1) Hyper-Raman PAP. When the relatively weak dump pulses transfer populations to the target state, the strong pump field is turned off. As a result, the levels are not Stark-shifted away from the dump resonance. Stark shifts are still present during each pump segment, introducing an additional relative phase to the state amplitudes.

We set the center wavelength of the pump field to 796 nm (instead of the resonant

wavelength of 777 nm) to compensate for the average shift of the levels during the pump segments. An offset in the dump frequency is only needed to compensate for the relative phase between the states $|2\rangle$ and $|3\rangle$ acquired during one pump pulse. Thus the probability of the successful transfer is a periodic function of the dump detuning with the period $2\pi/T$, where T is the delay between the individual pulses. This can be seen in Fig. 4.4(b) where the final population of the target state is shown as a function of the dump detuning. For comparison, we show the same dependance for the reference STIHRAP with smooth pulses[2]. One can see that the conditions for a successful implementation of a (2+1) PAP are drastically different from those for a conventional (2+1) STIHRAP: instead of carefully matching the detuning with the Stark shifts [16], the field has to satisfy the Ramsey-type condition within the bandwidth of a single pulse. Further studies are underway in order to find out whether (2+1) PAP can prove to be a practical tool for robust hyper-Raman transfer. The possibility to cancel an arbitrary Stark shift by a combination of the pump and dump detunings with additional delays [17] are of particular interest.

4.7 Remarks

In piecewise adiabatic passage, the alternating operators for the pump and dump transitions may be of quite general nature, and may act in a Hilbert space that is much larger than that spanned by three states. The states themselves are not required to be non-degenerate, nor even energy eignestates of the system. The only necessary requirements are that each pump operator transfers a fraction of population between an initial and some intermediate state, each dump operator transfers population between that intermediate and some desired target state, and that the coherence between the three states is preserved throughout the process. This may suggest a variety of new applications combining the robustness of the piecewise AP with various coherent control schemes with shaped femtosecond pulses.

[2]For proper comparison (see Eq.(4.5)), the values of the dump field, the pump intensity, and the frequency offset of the pump in the conventional STIHRAP were set to one fourth of those for the (2+1) PAP.

4.7.1 Quantum Computation with Femtosecond Pulses?

In relation to the quantum gate operations discussed in the previous chapter, it was our hope that a robust scheme involving femtosecond pulses as the one developed here would be able to shorten the computational time duration on the qubits. However, the PAP process must obey a coarse-grained adiabaticity condition which is nearly identical to that for the original prototype STIRAP. Thus the total duration of each femtosecond pulse train must be on the same order as the duration of the signal picosecond pulse. The product of the total number of individual pulses with each of their durations cannot be reduced below the threshold value given approximately by the length of the single long pulse which define the trains' global profile; this ensures that adiabaticity of the process. Additionally, since the use of femtosecond pulses results in a larger bandwidth, the isolated addressibility of a single qubit state, which is crucial to obtaining high fidelity rates in our logic operations, becomes very difficult. As a result, the application of PAP in performing the universal gate operations in the sodium dimer system gives efficiencies far from the necessary fault-tolerant threshold.

Chapter 5

Conclusions

The present thesis introduces a novel population transfer scheme known as adiabatic passage. The method has been shown to control not only the flow of population between states in multi-dimensional systems but also the ability to manipulate the phases of the target states. Following from its adiabatic nature, the procedure is endowed with robustness with respect to the experimental parameters, leading to its versatility which naturally lends itself to applications involving quantum information processing. One of the primary obstacles in quantum computing lies in the difficulty to complete precise logic operations on the system of qubits whilst avoiding the undesirable effects that cause decoherence of the system. The foreseen benefits of quantum computations rely in the fact that the coherence and entanglement of the qubits is maintained through an algorithm, and is not endangered by clumsy control procedures or the relaxation or decay of the states encoding the quantum information. The high contollability and accurate addressability of an APT scheme yields itself as a solution to these problems, where a series of gate operations can be carried-out on the quantum states before the system's coherence becomes affected.

A review of the famed STIRAP procedure is presented in Chapter 2 as applied to a three-level system in the Λ configuration. This section provides an outline of the theory describing the prototypical population transfer process by which the logic gates in the following chapter are preformed, and acts to facilitate the understanding of the more complex four-level adiabatic passage process developed later. The latter part of the chapter provides the reader with an overview of quantum computing in general, specifically focusing on the ingredients of a universal gate set. The two-state Bloch sphere fomulation is introduced as a means to conceptualize the single-qubit operations; this construct becomes particularly

insightful for the implementation of the Hadamard gate

In Chapter 3, a platform for quantum computation based upon encoding the qubits in the rovibrational eigenstates of a sodium molecule is considered. Ab-initio calculated electronic energy manifolds for the sodium dimer are used, together with a finite difference subroutine, to produce the eigenenergies and necessary coupling parameter for the molecular system. The single-qubit phase and Hadamard gates are demonstrated on a one-qubit system with nearly perfect fidelity. A rovibraional state residing in an excited potential energy surface serves as the intermediate level providing the required connection between the qubit levels and the additional shelving state. Using a similar encoding scheme for the two-qubit system, the controlled-NOT gate and a series of composite gate operations are simulated, with fidelities reaching above the presumed threshold for fault-tolerant quantum computing.

Drawbacks of using an APT scheme stem from its necessity to fulfill the adiabaticity conditions. Often this requirement restricts the bandwidth of the used pulses by instating a limit on the rate of the process. The possibility of combining the speed and pulse-shaping characteristics of coherent control with robustness of AP were studied. Hope lays in the potential of accelerating quantum computations similar to those shown here through the application of femtosecond pulses. A new scheme was developed which, although it did not present any obvious advantages towards performing quantum operations, opened-up a realm of new opportunities. The new control method, so-called piecewise adiabatic passage, was detailed in Chapter 4. Using the traditional stimulated Raman adiabatic passage scheme in a three-level Λ system as a reference process, the PAP procedure involved decomposing each of the long narrow-band pulses into a series a femtosecond pulses. Due to local experimental interests, numerical demonstrations were carried out with atomic sodium. It was found that when compared to the prototypical STIRAP process, PAP achieves nearly the same accuracy whilst retaining robustness ensured that the corresponding conditions for adiabacitiy are met. A rough theoretical explanation, as so far developed, is given using shake-off perturbation theory with the idea of a coarse-gained evolution. A classical analogue relating to the methodology of the process provides the reader with an alternate perpective, and

illustrates the point that this is not necessarily a quantum effect. An application of PAP is shown in relation to the Ramsey interference effect, as expected it is found that the longer pulse trains produce sharper Ramsey fringes. Secondly, advantages of PAP over the ordinary "2+1" Stimulated Hyper-Raman Adiabatic Passage method are considered with the intent that it may be able to greatly reduce the deleterious effects of the Stark shifts. An increase in the population transfer efficiency was noticed; however more studies are underway to determine its pratical feasibility.

I believe that there is a great potential in the applicability of the two broad ideas discussed in this thesis. The first scheme, which involves performing a robust operation of a universal set of logic gates for quantum computation using adiabatic poulation transfer between molecular levels, can be beneficial within other quantum computing platforms. It would be interesting to investigate alternate computational architectures, such as a series of atoms or molecules in optical cavities or arrays of electrons trapped in quantum wells, to determine the possibility of using these gate operations given their energy structure. The second idea resulted from the attempt to merge two of the most useful strategies which have emerged over the past decade for achieving quantum control. Although still in its infancy, the merits of PAP have begun to take form. It appears to me that if any general broad range control scheme were to be developed that it will result from a marriage between adiabatic passage and coherent control theory, perhaps eventually leading to an adiabatic optimal control approach.

Finally, a lot of recent studies have been directed towards manipulating the geometric phases of states over an adiabatic evolution as the means of performing a quantum control; this has most prominently been detailed in the context of holonomic quantum computing. It would be interesting to research the possibility of combining this in conjuncture with the previously mentioned approaches. One immediate application may be to offset dynamical phase evolution of non-degenerate states in a quantum computation.

Bibliography

[1] A.M.Weiner. Femtosecond pulse shaping using spatial light modulators. *Rev. Sci. Inst.*, 71:1929, 2000.

[2] D. Babikov. *J. Chem. Phys.*, 121:16, 2004.

[3] A. Barenco, D. Deutsch, A. Ekert, and R. Jozsa. Conditional quantum dynamics and logic gates. *Physical Review Letters*, 74(20):4083, 1995.

[4] Benjamin Bederson and Herbert Walther. *Atomic, Molecular and Optical Physics*, volume 46. Academic Press, 2001.

[5] K. Bergmann, H. Theuer, and B.W. Shore. *Rev. Mod. Phys.*, 70:1003, 1998.

[6] Asoka Biswas. PhD thesis, Gujarat University, Ahmedabad, India, 2004.

[7] P.O. Boykin, T. Mor, M. Pulver, V. Roychowdhury, and F. Vatan. *Information Processing Letters*, 75(3):101, 2000.

[8] V. P. Bykov. Laser investigation and quantum theory. *Journal of Russian Laser Research*, 18(3):260, 1997.

[9] J.J. Camacho, A. Pardo, and J.M.L. Poyato. *J. Phys. B*, 38:1935, 2005.

[10] A.M. Childs, E. Farhi, and J. Preskill. *Phys. Rev. A*, 65:012322, 2001.

[11] W. Demtröder, W. Stetzenback, M. Stock, and J. Witt. *J. Mol. Spectrosc.*, 61:382, 1976.

[12] D.Villeneuve and et al. *Physical Review Letters*, 85:542, 2000.

[13] A.M. Dykhne and G.L. Yudin. Jarring of a quantum system and the corresponding stimulated transitions. *Sov. Phys. Uspekhi*, 21:549, 1978.

[14] A. Einstein. Zur quantentheorie de strahlung. *Phys. Z.*, 18:121, 1917.

[15] K. Böhmer et.al. Stimulated hyper-raman ap. iii: Experiment. *Physical Review A*, 64(023404), 2001.

[16] S. Guérin et.al. Stihrap. ii: Static compensation of dynamic stark shifts. *Physical Review A*, 58:4691, 1998.

[17] T. Zonon-Willette et.al. *Physical Review Letters*, 97(233001), 2006.

[18] Edward Farhi and et al. *Science*, 292:472, 2001.

[19] B. Furrow. A panoply of quantum algorithms. Master's thesis, University of British Colombia, Vancouver, 2006. quant-ph/0606127v1.

[20] U. Gaubatz, P.Rudecki, S. Schiemann, and K. Bergmann. *J. Chem. Phys.*, 92:5363, 1990.

[21] H. Goldstein. *Classical Mechanics.* Addison-Wesley, 2nd edition, 1980.

[22] H. Goto and K. Ichimura. *Phys. Rev. A*, 70:012305, 2004.

[23] D. Gottesman. PhD thesis, Caltech, Pasadena, 1997. e-print quant-ph/9705052.

[24] M. Granjcar, A. Izmalkov, and E. Il'ichev. *Phys. Rev. B*, 71:4450, 2005.

[25] David J. Griffiths. *Introduction to Quantum Mechanics.* Prentise Hall Inc., 1 edition, 1995.

[26] Lov K. Grover. A fast quantum mechanical algorithm for database search. *e-print arXiv:quant-ph/9605043v3*, 1996.

[27] S. Guérin and A. Jauslin. Two-laser multiphoton passage in the frame of the floquet theory. *Euro. Phys. J. D.*, 2:99, 1998.

[28] F.T. Hioe. N-level system with su(2) dynamic symmetry. *J. Opt. Soc. Am. B*, 4:1327, 1987.

[29] V. Hughes and L. Grabner. *Phys. Rev.*, 79:5, 1950.

[30] K.M Jones, S. Maleki, S. Bize, P.D. Lett, C.J. Williams, H. Richling, H. Knöchel, E. Tiemann, H. Wang, P.L. Gould, and W.C Stwalley. *Physical Review A*, 54:1006, 1996.

[31] W.M. Kaminsky, S. Lloyd, and T.P. Orlando. *e-print quant-ph/0403090*, 2005.

[32] Z. Kis and F. Renzoni. *Phys. Rev. A*, 65:032318, 2002.

[33] E. Knill. *Nature*, 434:39–44, 2005.

[34] P. Král, I. Thanopulos, and M. Shapiro. Coherently controlled adiabatic passage. *Review of Modern Physics*, 79:53, 2007.

[35] K.Xu, T. Mukaiyama, J.R. Abo-Shaeerand, J.K. Chin, D.E. Miller, and W. Ketterle. *Phys. Rev. Lett.*, 91:210402, 2003.

[36] D. Lucarelli. *J. Math. Phys.*, 46:052103, 2005.

[37] C. Menzel-Jones and M. Shapiro. *Physical Review A*, 75(1), 2007.

[38] M. A. Nielson and I. L. Chuang. *Quantum Computation and Quantum Information.* Cambridge University Press, Cambridge, 2000.

[39] J. Oreg, F.T. Hioe, and J.H. Eberly. Adiabatic following in multilevel systems. *Phys. Rev. A*, 29:690, 1984.

[40] J.P. Palao and R. Koslof. *Phys. Rev. A - Erratum*, 69:059901, 2004.

[41] J.P. Palao and R. Kosloff. *Phys. Rev. Lett.*, 89:188301, 2002.

[42] J.P. Palao and R. Kosloff. *Phys. Rev. A*, 68:062308, 2003.

[43] P.Král, Z. Amitay, and M. Shapiro. An analytic solution of the non-degenerate quantum control problem. *Physical Review Letters*, 89(063002), 2002.

[44] John Preskill. Fault-tolerant quantum computation. *e-print quant-ph/9712048v1*, 1997.

[45] W.H. Press, S.A. Teukolsky, W.T. Vetterling, and B.P. Flannery. *Numerical Recipes in Fortran 77*, volume 1. Cambridge University Press, 2nd edition, 1992.

[46] A.K. Prykarpatsky. *Conference on Geometry and Topology of Manifolds*, 4:April 28, 2002.

[47] N.F. Ramsey. A molecular beam resonance method with separated osciallating fields. *Physical Review*, 78:695, 1950.

[48] S.A. Rice and M. Zhao. *Optical Control of Molecular Dynamics.* Wiley-Interscience, New York, 2000.

[49] V.I. Romanenko and L.P. Yatsenko. Simulated raman adiabatic passage in fields with stochastic amplitudes. *J. Exp. Theor. Phys.*, 101:913, 2005.

[50] N. Sangouard, X. Lacour, S. Guérin, and H.R. Jauslin. *Phys. Rev. A*, 72:062309, 2005.

[51] N. Sangouard, X. Lacour, S. Guérin, and H.R. Jauslin. *Eur. Phys. J. D*, 37:451, 2006.

[52] M.S. Sarandy and D.A. Lidar. *Phys. Rev. Lett.*, 95:250503, 2005.

[53] Ilona Schmidt. Eigenschaften angeregter zustände der alkalidimeren li_2, na_2 und nali sowie deren kationen aus ab-initio-rechnungen. Master's thesis, Universität Kaiserlautern, Kaiserslautern, 1987.

[54] E.A. Shapiro, V. Milner, C. Menzel-Jones, and M. Shapiro. *Physical Review Letters*, 99(033002), 2007.

[55] M. Shapiro and P. Brumer. *Principles of the Quantum Control of Molecular Processes.* John Wiley Sons Inc., New Jersey, 2003.

[56] S. Shi, A. Woody, and H. Rabitz. *J. Chem. Phys.*, 88:6870, 1988.

[57] Peter Shor. Fault-tolerant quantum computation. In *Proceedings of the Symposium on the Foundations of Computer Science.* (Los Alamits, CA: IEEE Press, e-print quant-ph/9605011v1, 1996.

[58] Peter W. Shor. Polynomial-time algorithms for prime factorization and discrete logarithms on a quantum computer. *e-print arXiv:quant-ph/9508027v2*, 1997.

[59] Bruce W. Shore. *The Theory of Coherent Atomic Excitation.* Wiley, 1990.

[60] A. Steane. *Physical Review A*, 68(042322), 2003.

[61] M. Steffen and et al. *Phys. Rev. Lett.*, 90:067903, 2003.

[62] W.J. Stevens and et al. *Journal of Chemical Physics*, 66:1477, 1977.

[63] M.C. Stowe and et al. High resolution atomic coherent control via... *Physical Review Letters*, 96(153001), 2006.

[64] D.J. Tannor and S.A. Rice. *J. Chem. Phys.*, 92:5013, 1985.

[65] C.M. Tesch and R. de Vivie-Riedle. *J. Chem. Phys.*, 121:24, 2004.

[66] L.P. Yatsenko *et. al.*. Simulated hyper-raman adiabatic passage. *Physical Review A*, 58:4683, 1998.

[67] H. Theuer, R.G.Unanyan, C. Habschied, K. Klein, and K. Bergmann. *Opt. Express*, 4, 1999.

[68] U. Troppman and R. de Vivie-Riedle. *J. Chem. Phys.*, 122:154105, 2005.

[69] U. Troppmann, C.M. Tesch, and R. de Vivie-Riedle. *Chem. Phys. Lett.*, 378:273, 2003.

[70] R.G. Unanyan, M. Fleischhauer, B.W. Shore, and K. Bergmann. *Opt. Commun.*, 155, 1998.

[71] A. Vardi and M. Shapiro. Two photon dissociation/ionization beyond the adiabatic approximation. *Journal of Chemical Physics*, 104:5490, 1996.

[72] Nikolay V. Vitanov, Thomas Halfmann, Bruce W. Shore, and Klass Bergmann. Laser-induced population transfer by adiabatic passage techniques. *Annual Reviews Physical Chemistry*, 52:763–809, 2001.

[73] N.V. Vitanov, M. Fleischhauer, B.W. Shore, and K. Bergmann. *Adv. At. Mol. Opt. Phys.*, 46:55, 2001.

[74] M. Wollenhaupt, V. Engel, and T. Baumert. Femtosecond laser photoelectron spectroscopy on atoms and small molecules: Prototypical studies in quantum control. *Annual Review Physical Chemistry*, 56:25–56, 2005.

[75] M. Wollenhaupt and et al. Femtosecond strong-field quantum control with sinusoidally phase-modulated pulses. *Physiccal Review A*, 73(063409), 2006.

[76] L.-A. Wu, P. Zanardi, and D.A. Lidar. *Phys. Rev. Lett.*, 95:130501, 2005.

[77] L.P. Yatsenko and et al. Simulated raman adiabatic passage with amplitude modulated fields. *Eur. Phys. J. D.*, 4:47, 1998.

[78] J. Ye and S.T. Cundiff. *Femtosecond optical frequency comb technology: principle, operation, and applications.* Springer, 2005.

[79] P. Zanardi and M. Rasetti. *Phys. Lett. A*, 264:94, 1999.